

MASSIV: Mass Assembly Survey with SINFONI in VVDS \star

IV. Fundamental relations of star-forming galaxies at $1 < z < 1.6$ $\star\star$

D. Vergani^{1,2}, B. Epinat^{3,4,5}, T. Contini^{3,4}, L. Tasca⁵, L. Tresse⁵, P. Amram⁵, B. Garilli⁶, M. Kissler-Patig⁷, O. Le Fèvre⁵, J. Moutata^{3,4}, L. Pajor⁶, J. Queyrel^{3,4}, and C. López-Sanjuan⁵

¹ INAF-IASFBO, Via P. Gobetti 101, I-40129 Bologna, Italy, e-mail: vergani@iasfbo.inaf.it

² INAF-Osservatorio Astronomico di Bologna, Via C. Ranzani 1, I-40127 Bologna, Italy

³ Institut de Recherche en Astrophysique et Planétologie (IRAP), CNRS, 14 Avenue Édouard Belin, F-31400 Toulouse, France

⁴ IRAP, Université de Toulouse, UPS-OMP, F-31400 Toulouse, France

⁵ Laboratoire d’Astrophysique de Marseille, Université d’Aix-Marseille, CNRS, 38 rue Frédéric Joliot-Curie, F-13388 Marseille Cedex 13, France

⁶ INAF-IASFMI, Via E. Bassini 15, I-20133 Milano, Italy

⁷ ESO, Karl-Schwarzschild-Str. 2, D-85748 Garching b. München, Germany

Received 14 November 2011 / accepted 14 February 2012

ABSTRACT

Aims. How mass assembly occurs in galaxies and which process(es) contribute to this activity are among the most highly debated questions in galaxy formation and evolution theories. This has motivated our survey MASSIV (Mass Assembly Survey with SINFONI in VVDS) of $0.9 < z < 1.9$ star-forming galaxies selected from the purely flux-limited VVDS redshift survey.

Methods. We evaluate the characteristic size and stellar mass of 46 MASSIV galaxies at $1 < z < 1.6$ and use the internal dynamics obtained with the SINFONI integral field spectrograph mounted at the Very Large Telescope.

Results. For the first time, we derive the relations between galaxy size, mass, and internal velocity, and the baryonic Tully-Fisher relation, from a statistically representative sample of star-forming galaxies at $1 < z < 1.6$. We find a dynamical mass that agrees with those of rotating galaxies containing a gas fraction of $\sim 20\%$, that is perfectly consistent with the content derived using the Kennicutt-Schmidt formulation and corresponds to the expected evolution. Non-rotating galaxies have more compact sizes for their stellar component, and are less massive than rotators, but do not have statistically different sizes for their gas-component. Discs of ionized gas have irregular, clumpy distributions, but the simplistic assumption of exponential profiles is verified. We measure a marginal evolution in the size - stellar mass and size - velocity relations in which discs become evenly smaller with cosmic time at fixed stellar mass or velocity, and are less massive at a given velocity than in the local Universe. This result is inconsistent with previous reports of an abnormal evolution in the galactic spin. The scatter in the Tully-Fisher relation is smaller when we introduce the S_{05} index, which we interpret as evidence of an increase in the contribution to galactic kinematics of turbulent motions with cosmic time. We report a persistently large scatter for rotators in our relations, that we suggest is intrinsic, and possibly caused by complex physical mechanism(s) at work in our stellar mass/luminosity regime and redshift range.

Conclusions. Our results consistently point towards a mild, net evolution of these relations, comparable to those predicted by cosmological simulations of disc formation. In a conflictual picture where earlier studies reported discrepant results, we place on firmer ground the measurement of a lack of any large evolution of the fundamental relations of star-forming galaxies in at least the past 8 Gyr and evidence that dark halo is strongly coupled with galactic spectrophotometric properties.

Key words. Galaxies: high-redshift - galaxies: evolution - galaxies: kinematics and dynamics - galaxies: fundamental parameters

1. Introduction

In the current paradigm of structure formation, galaxies are formed in dark matter halos that grow with cosmic time via the hierarchical assembly of smaller units. While halo-halo merging is the main physical process driving the assembly of

dark-matter halos and successfully describes the galaxy clustering properties, it is unclear how it affects the build-up of galaxies, and how other physical processes might play a role.

Large and deep spectroscopic surveys of local and higher- z galaxies have been performed in the past decade to improve our understanding of galaxy formation and evolution. Among the many trends that have been found between various galaxy properties (e.g., luminosity, colour, stellar mass, surface brightness, and star-formation rate), a general consensus has been reached on a luminosity/mass-dependent evolution of the distribution functions (e.g. Zucca et al. 2006; Pozzetti et al. 2007; Bundy et al. 2006; Fontana et al. 2004, 2006) supporting the downsizing scenario (e.g. Cowie et al. 1996).

There is convincing evidence that $1 < z < 2.5$ is a critical cosmic period, when galaxy properties changed rapidly. During this period, we understand that there was an intense

Send offprint requests to: D. Vergani, e-mail: vergani@iasfbo.inaf.it

\star This work is based mainly on observations collected at the European Southern Observatory (ESO) Very Large Telescope, Paranal, Chile, as part of the Programs 179.A-0823, 177.A-0837, 78.A-0177, 75.A-0318, and 70.A-9007. This work also benefits from data products produced at TERAPIX and the Canadian Astronomy Data Centre as part of the Canada-France-Hawaii Telescope Legacy Survey, a collaborative project of NRC and CNRS.

$\star\star$ All the data published in this paper are publicly available following this link: <http://cosmosdb.lambrate.inaf.it/VVDS-SINFONI>

mass assembly activity and that the morphological distinction between galaxies became established. This epoch corresponds to the maximal star formation activity in the Universe around $z \sim 2$ (e.g. Tresse et al. 2007; Cucciati et al. 2012), and the rapid build-up of the stellar mass observed in early-type galaxies at $z \sim 1-1.5$ (Arnouts et al. 2007; Vergani et al. 2008). It is also an epoch when the connection between AGN activity and star formation might have played an important role in shaping galaxies. In this framework, knowledge of the dynamical state of galaxies is indispensable to assessing the mechanisms governing the growth of luminous structures in the Universe.

In the past few years, the availability of integral field spectrographs working under excellent seeing conditions, or assisted by adaptive optics, has opened a new era in the investigation of galactic resolved dynamics at high redshifts, with integral field spectrographs providing considerably more information than traditional long-slit techniques. Acquiring the full two-dimensional maps of both the velocity fields and velocity dispersions is far more helpful to many dynamical studies than the classical long-slit technique because it avoids any misinterpretation of the measured velocities due to either the misalignment between the photometric and kinematic axes, or large velocity dispersions. This is especially true at increasingly large look-back times when galaxies display a larger incidence of irregular shapes and chaotic motions. In addition, new opportunities have recently been arisen in the near-infrared regime in which new instruments allow one to sample the rest-frame optical emission that contains all major diagnostic lines, e.g., SINFONI on the Very Large Telescope (VLT), Eisenhauer et al. (2003) and OSIRIS on Keck, Larkin et al. (2006). Spatially-resolved observations of UV/optically selected galaxies at $1.5 < z < 3$ (Genzel et al. 2006, 2008; Förster Schreiber et al. 2006; Förster Schreiber et al. 2009; Bouché et al. 2007; Law et al. 2007, 2009; Wright et al. 2008; Stark et al. 2008; Epinat et al. 2009) together with cosmological simulations (e.g., Genel et al. 2008; Dekel et al. 2009) indicate that many of the physical properties of these sources cannot be primarily attributed to major merger events experienced in the history of galaxies. Internal mechanisms instead contribute to mass assembly (Genzel et al. 2008, and references therein). In determining the observed dynamics, these processes might correspond to the infall of accreting matter, and/or large collisional clumps (e.g., Law et al. 2007, 2009; Genzel et al. 2011) and/or processes related to star formation (Lehnert et al. 2009).

In summary, the emerging scenario places a far smaller importance on major merging in shaping up galaxies at early epochs, apparently at odds with the hierarchical assembly of mass in the cold dark matter paradigm - although merging systems have been identified in about one third of the galaxies studied. A general consensus has yet to be reached (e.g., Robertson & Bullock 2008).

To date a detailed view of dynamics of distant galaxies has been restricted to a limited number of objects primarily because of the large investment of telescope time required to build up a fair sample. The most efficient approach has been to adopt certain selection techniques, such as various combinations of colours to focus on a specific redshift range and/or target extended discs to ensure sufficient spatial sampling (Law et al. 2007, 2009; Förster Schreiber et al. 2006; Förster Schreiber et al. 2009). While pre-selecting galaxies remains the most effective way to ensure the production of a large, high- z galaxy catalogue, when exploring statistical issues it is highly desirable to have a fully representative catalogue of galaxies with well-known selection functions in multiple fields of a

homogeneous survey (e.g., Puech et al. 2010). The importance of a sufficient spatial resolution has also been demonstrated by surveys such as IMAGES (Intermediate MAss Galaxy Evolution Sequence), which selects $z \sim 0.6$ galaxies observed with limited spatial resolution ($0''.52 \text{ pix}^{-1}$). The resulting picture emerging from various data-sets provides discrepant results about the evolution of the fundamental relations between galaxy size, mass, and velocity (e.g., Flores et al. 2006; Puech et al. 2008, 2010; Bouché et al. 2007; Förster Schreiber et al. 2009; Cresci et al. 2009; Law et al. 2007, 2009). As these quantities represent important indicators of the structure and evolution of disc galaxies, the interpretation of their changes, or constancy with time, helps us to determine the standard picture of galaxy disc formation. For instance, at odds with earlier findings and theoretical expectations, the absence of any evolution in the size-velocity relation of disc galaxies, as reported by Bouché et al. (2007), has fundamental implications for the growth of the specific angular momentum of dark matter halos.

To overcome the aforementioned difficulties and shed light on relations linking various galactic properties to dynamics, we are carrying out the MASSIV programme (Mass Assembly Survey with SINFONI in VVDS) to obtain near-infrared integral field spectroscopy of a hundred star-forming galaxies selected by applying a pure flux-limit criterion to three VVDS fields. The main goal of MASSIV is to obtain a detailed description of galaxy dynamics to probe their formation and evolution for a representative sample of galaxies in the crucial $1 < z < 2$ epoch. In the first set of papers, we present the survey in Contini et al. (2012), the kinematic classification of galaxies in Epinat et al. (2012), and the resolved metallicity data of galaxies in Queyrel et al. (2011). In the present paper, we present the fundamental scaling relations that exist among the mass, size, and velocity of the studied galaxies.

In Sect. 2, we summarize our sample selection, observations, and data reduction. In Sect. 3, we detail the procedures to determine the physical properties of the MASSIV galaxies (morphology, mass, star formation rate, and kinematics inferred from the photometric and integral field spectroscopic data). In Sect. 4, we discuss the gas contents and sizes of our galaxies, and in Sect. 5, we analyse our resulting scaling relations in the context of mass assembly.

Throughout this work, we assume a standard cosmological model with $\Omega_M = 0.3$, $\Omega_\Lambda = 0.7$, and $H_0 = 70 \text{ km s}^{-1} \text{ Mpc}^{-1}$ (which gives a median scale of $8.32 \text{ kpc arcsec}^{-1}$ at $z \sim 1.24$). Magnitudes are given in the AB system.

2. Observations

2.1. Sample selection

We report SINFONI (Eisenhauer et al. 2003; Bonnet et al. 2004) observations of our new resolved kinematic MASSIV survey. The observed galaxies were selected from the VVDS. The VVDS is a redshift survey that has presented results on the evolution of galaxies, large-scale structures, and AGNs based on the spectroscopic identification of about 50,000 sources down to a limiting magnitude of $I_{AB} = 22$ in the wide fields (Garilli et al. 2008), to $I_{AB} = 24$ in the deep field (Le Fèvre et al. 2005), and to $I_{AB} = 24.75$ in the ultra-deep field (see Tab. 1). The VVDS has been combined with a multi-wavelength dataset from radio to X-rays.

The MASSIV sample analysed in this work was selected based on several criteria (see details in Contini et al. 2012), which can be summarized as follows:

1) Galaxies with a redshift assigned to their rest-frame UV VVDS spectra at a confidence level higher than 80% in the redshift range $z = 0.9 - 1.8$ were pre-selected. The confidence level of the redshift determination had been estimated in the VVDS based on repeated observations. Galaxies were grouped into four classes and we used only those that corresponded to the maximum success probability of having an accurate redshift.

2) Their spectral features ($\text{H}\alpha\lambda 6563\text{\AA}$ or $[\text{OIII}]\lambda 5007\text{\AA}$) had to fall in a region not contaminated by OH sky-lines. Strong sky-lines were outdistanced by a minimum of 9\AA from the above-mentioned spectral lines computed using our VIMOS spectroscopic redshifts. Thus, we could observe an OH-uncontaminated emission line with a typical rotation of 200 km s^{-1} .

3) Star-forming galaxies at redshifts $z < 1.46$ were selected by taking a certain threshold in the equivalent width (EW) of the $[\text{OII}]\lambda 3727$ doublet in VIMOS spectra with a signal-to-noise ratio (S/N) above 6. Hence, we selected $z < 1.46$ galaxies with $\text{EW}[\text{OII}]$ larger than 25\AA in $\text{S/N} \leq 10$ spectra and 40\AA in $6 \leq \text{S/N} \leq 10$ spectra. Star-forming galaxies at higher redshifts were selected based on the rest-frame UV spectra. These constraints guarantee the detection of $\text{H}\alpha\lambda 6563\text{\AA}$ (or $[\text{OIII}]\lambda 5007\text{\AA}$) in SINFONI spectra within the scheduled observing time.

Out of the $\sim 30,000$ spectra observed in the various VVDS fields, 10% of them satisfy these criteria (see Tab. 1 for the details). From this subsample, 84 galaxies have been observed in the framework of MASSIV. The galaxy VVDS220148046, which had been assumed to be at redshift 1.3710 based on its VIMOS spectrum, turns out to have a redshift of 2.2442 identified with the $\text{H}\beta$ and $[\text{OIII}]$ lines in SINFONI observations. This galaxy is not included in the current analysis. Finally, our 83 galaxies are representative of a star-forming galaxy population at $0.9 < z < 1.8$ that is uniformly distributed in the stellar mass interval $\log M/M_\odot = 9.47 - 11.77$. In this sample, ten galaxies have been observed with the adaptive optics (AO) system of SINFONI assisted with the Laser Guide Star (LGS) facility to achieve a higher angular resolution.

In this analysis, we use more than half of the entire MASSIV sample, i.e., 50/83 galaxies, or about $\sim 60\%$. Thanks to the high precision of the VVDS redshifts, almost all observed galaxies have been detected (45/50) using either the $\text{H}\alpha\lambda 6563\text{\AA}$ (44/45) or $[\text{OIII}]\lambda 5007\text{\AA}$ (1/45) spectral lines. In particular, in seeing-limited mode all but one (43 out of 44) of the galaxies targeted

in $\text{H}\alpha\lambda 6563\text{\AA}$ have been detected. Seven out of 50 galaxies have been observed with adaptive optics (among which two have no detection, and one was targeted in $\text{H}\alpha$ while another was targeted in $[\text{OIII}]$). The 50 galaxies that constitute the original MASSIV sample (see Tab. 1) have a median redshift of $z = 1.2423$ (where $z_{25\%} = 1.0375$ and $z_{75\%} = 1.3547$ are the two extreme quartiles of the redshift distribution). Excluding our serendipitous detection at $z = 2.2442$ and the four undetected galaxies, the median redshift of our 45 galaxies analysed in this work remains similar to that of the original sample ($z = 1.2246$ with $z_{25\%} = 1.0351$ and $z_{75\%} = 1.3338$).

2.2. SINFONI data acquisition and reduction

Our observations of the MASSIV sample were collected with the near-infrared integral field spectrograph SINFONI of the VLT under the large programme 179.A-0823 (P.I. T. Contini) between April 2007 and January 2011 and include the observations of the pilot runs 75.A-0318 and 78.A-0177. Our subsample of 50 galaxies refers to observations conducted until 2009 and fully reduced and analyzed before 2010.

In the accompanying paper by Contini et al. (2012), we detail the strategy and global physical properties of MASSIV galaxies, along with a more exhaustive explanation of selection functions. A full description of the data reduction procedures are given in Epinat et al. (2012). Here we provide a short summary.

We used the J- and H-bands to sample the spectral interval $1.08 - 1.41 \mu\text{m}$ and $1.43 - 1.86 \mu\text{m}$ with a spectral resolution of $R \sim 2000$ and ~ 3000 , respectively. The majority of our observations were in seeing-limited mode with a $8'' \times 8''$ field-of-view and $0''.125 \times 0''.25$ pixel scale. For a subsample of seven galaxies, we obtained AO observations with a $3''.2 \times 3''.2$ field-of-view and $0''.100 \times 0''.050$ pixel scale. To maximize the telescope time, we placed the majority of our targets at different positions in the field-of-view of the instrument. This strategy avoids the need for sky frame acquisition (for detail see in Contini et al. 2012). In addition, we applied a sub-dithering to place the target at different positions on the chip. Conditions were photometric during the observations with a median seeing of $0''.70$ measured using observations of the stars acquired to measure the point spread function (PSF) during the night. To accurately point our galaxies, we acquired them by performing a blind offset from a bright nearby star. We also observed standard stars over the same nights to enable us to flux-calibrate our spectra. Individual exposures ranged between 300s and 900s with a total on-source integration time that ranged between 1h and 2h.

The core of the data reduction was performed using the ESO-SINFONI pipeline, version 2.0.0 (Modigliani et al. 2007) complemented with additional routines to homogenize the data processing among the different reducers. We subtracted the sky background, skylines, and dark current from the raw science data using the contiguous sky frames obtained with the offset-to-sky sequence. The data were flat-fielded using observations of an internal lamp that had been wavelength calibrated with spectra of reference arc-lamps. These processed data frames were then reconstructed into data cubes. Individual cubes of a given observing block were aligned in the spatial direction by relying on the telescope offsets from a nearby bright star, and then combined. The rejection of cosmic rays was applied to the combined cubes. The observations of a telluric standard star of a typical B spectral type were acquired immediately after each science frames and were reduced in a similar way. We extracted the mono-dimensional spectra of the stars by summing the flux of an aperture of a diameter of five resolution elements to derive

Table 1. Sample selection.

VVDS Survey fields	$I_{AB,\text{lim}}$	Number of targets	Criteria	MASSIV sample	This work
(1)	(2)	(3)	Full-filled	(5)	(6)
Wide	17.5-22.50	24,507	224 (183)	21 (4)	21 (4)
Deep	17.5-24.00	12,668	2,600 (300)	29 (1)	27 (1)
Ultra-Deep	23.0-24.75	1,200	86 (55)	34 (6)	2 (2)

(1) The fields of the VVDS used in MASSIV. (2) I_{AB} limiting magnitude selection. (3) Total number of spectroscopic targets. (4) Number of targets fulfilling the criteria described in Sect. 2.1. (5) Total number of galaxies in the MASSIV sample at the completion of the survey. (6) Number of galaxies used in this analysis. In columns (4) to (6), we indicate in parentheses the numbers of targets observed with adaptive optics in our observing campaign.

the flux calibration after removing the telluric absorption lines. We corrected for the atmospheric transmission dividing the science cubes by the integrated spectrum of the telluric standard. We created sky cubes to quantify the effective resolution for each science data cube. The sky cubes were reduced in a similar way to the science frames, but no correction for sky subtraction was applied. We fitted with Gaussian profiles the unblended night sky lines in the extracted, mono-dimensional spectra. The effective FWHM spectral resolution has a typical value of 130 km s^{-1} .

3. Derived quantities

3.1. Morphology and kinematics

We used the $\text{H}\alpha\lambda 6563\text{\AA}$ line (and $[\text{OIII}]\lambda 5007\text{\AA}$ line in one case) to derive the dynamical properties. We assumed that the ionized gas rotates in a thin disc with a velocity reaching a plateau in the outer regions (but for 8/23 rotating galaxies marked with ^(c) in column (9) of Tab. 2, this radius was not reached within the area covered by our observations). Using a χ^2 minimization, we produce seeing-corrected velocity and dispersion maps of galaxies with geometrical inputs weighted by the S/N of each pixel.

The input geometrical parameters of the fitting model were estimated from the I-band best-seeing CFHTLS¹ Megacam images for all galaxies, apart from 14^{hr} galaxies that were covered with the I-band CFHT-12K camera only (McCracken et al. 2003). At the typical $z \sim 1.2$ redshift of MASSIV galaxies, I-band images probe the $3200\text{-}4200\text{\AA}$ rest-frame wavelength range, or the U-band. We used the GALFIT software (Peng et al. 2002) that convolves a PSF with a model galaxy image based on the initial fitting parameter estimates determined by fitting a Sérsic (1968) profile. GALFIT converges into a final set of parameters such as the centre, the position angle, and the axial ratio. Residual maps from the fit were used to optimize the results. The I-band images were also used to calibrate for SINFONI astrometry, by considering the relative positions of the PSF star. GALFIT was also applied to the ionised gas maps (properly deconvolved with a PSF star) to derive the semi-major axis disc scale-length. The CFHT images and the kinematic maps are presented in Epinat et al. (2012), where more discussion is presented on the modelling procedure.

The major source of uncertainties in deriving the maximum rotation velocity is the inclination of the studied galaxy. For very small objects, the inclination is not robustly constrained, thus for a fraction of galaxies the median inclination value of a random distribution of galaxies on the sky (60°) is adopted instead. For this category of objects, we estimated that a typical uncertainty of 24° is associated with the inclination. Another uncertainty appears when the maximum velocity is not reached within the radius covered by our observations. Other uncertainties entering into the error budget are related to the simplistic disc model adopted. The evaluation of the net effects of this assumption would require some assumption about the different, detailed modelling schemes, which is beyond the scope of this paper. The final uncertainty associated with our velocities includes both the

errors originating from the deprojection of the radial velocity given a certain inclination (estimated with Monte Carlo simulations) and the errors in the modelling procedure (quantified using simulations of the GHASP local sample following Epinat et al. 2012).

3.2. Mass and star formation rate

We inferred the stellar mass from a spectral energy distribution (SED) fit to photometric and spectroscopic data with BC03 stellar population synthesis models (Bruzual & Charlot 2003) using the GOSSIP spectral energy distribution tool (Franzetti et al. 2008). We assumed a Salpeter initial mass function (Salpeter 1955) with a lower and upper mass cutoff of respectively 0.1 and $100M_\odot$, and a set of delayed exponential star formation histories with galaxy ages in the range from 0.1 to 15 Gyr. As input to the SED fitting, we used the multi-band photometric observations available in the VVDS fields, including BVRI data from the CFHT-12K camera, ugriz data from the CFHT Legacy Survey, J and Ks-band data from SOFI at the NTT, from the UKIDSS survey, SWIRE data when available, and the VVDS spectra. Following Walcher et al. (2008), we adopted the probability distribution function to obtain the stellar mass (listed in column (6) of Tab. 2), the absolute magnitude, and other results of the fitting procedure as detailed in Contini et al. (2012).

We estimated the dynamical mass and the gas mass in our galaxies to trace the evolution of both the baryonic and dark matter components. As described in the next section our galaxies have a variety of kinematical properties that we classify into two broad categories: rotating and non-rotating systems (see details in Sect. 3.3 of this paper and Epinat et al. 2012). The dynamical mass is estimated using the equation

$$M_{\text{dyn}} = \frac{V^2 R}{G} + \frac{\sigma^2 R^3}{G h^2}, \quad (1)$$

where the first term represents the mass enclosed within the radius R defined as the total extent of the ionized gas, V is the velocity at the same radius, and G is the universal gravitational constant. The second term represents the asymmetric drift correction following Meurer et al. (1996), where σ is the dispersion velocity at R , and h is the gas disc scale length in an isotropic geometrical configuration with a surface density described by a Gaussian function. The dynamical mass of each galaxy is given in column (6) of Tab. 2, where its error was estimated by accounting for the uncertainties related to the inclination and the modelling procedure.

The gas mass was derived using the empirical correlation between star formation rate (SFR) and gas surface density assuming that the gas and the stellar content accounts for the majority of the mass in the central regions of galaxies. In the local Universe, Kennicutt (1998b) proved that the conversion of the surface density of gas to star-formation rate follows a power law above some critical gas density (Schmidt 1959, $\Sigma_{\text{SFR}} = A \Sigma_{\text{gas}}^n$) over more than six orders of magnitude in Σ_{SFR} . This empirical correlation has not yet been routinely proven to hold at high redshift because of the lack of extensive measurements of cold gas mass, but a number of studies of small samples support the validity of this relation at high redshifts (e.g., Erb et al. 2006; Bouché et al. 2007; Daddi et al. 2010; Tacconi et al. 2010). Some detailed studies of individual galaxies also highlight a consistency with the local Schmidt law (e.g., the lensed $z = 2.7$ LBG MS1512-cB58, Baker et al. 2004). Thus, we computed the star-formation rate surface densities using the total SFR and the size of our galaxies.

¹ Based on observations obtained with MegaPrime/MegaCam, a joint project of CFHT and CEA/DAPNIA, at the Canada-France-Hawaii Telescope (CFHT) which is operated by the National Research Council (NRC) of Canada, the Institut National des Science de l'Univers of the Centre National de la Recherche Scientifique (CNRS) of France, and the University of Hawaii. This work is based in part on data products produced at TERAPIX and the Canadian Astronomy Data Centre as part of the Canada-France-Hawaii Telescope Legacy Survey, a collaborative project of NRC and CNRS.

Table 2. PROPERTIES OF THE MASSIV SAMPLE

ID (1)	z (2)	Line (3)	M_* (4)	M_{gas} (5)	M_{dyn} (6)	R_{last} (7)	$R_{1/2,\text{gas}}$ (8)	$R_{1/2,\text{star}}$ (9)	V_{max} (10)	V_{max}/σ (11)	Class (12)
020106882	1.3991	$\text{H}\alpha$	$9.99^{+0.22}_{-0.22}$	9.84	$10.41^{+0.18}_{-0.13}$	5.1	3.79 ± 0.08	3.51 ± 0.14	133 ± 25	3.2	ROT
020116027	1.5302	$\text{H}\alpha$	$10.09^{+0.23}_{-0.23}$	9.86	$9.94^{+0.23}_{-0.29}$	6.5	3.56 ± 0.08	4.27 ± 0.16	27 ± 10	0.6	NON-R
020126402	1.2332 ^{a,b}	[OIII]	$10.09^{+0.26}_{-0.25}$	2.12 ± 0.31
020147106	1.5195	$\text{H}\alpha$	$10.10^{+0.13}_{-0.13}$	9.89	$11.73^{+0.36}_{-0.36}$	7.8	1.52 ± 0.08	1.17 ± 0.41	26 ± 51	0.3	ROT ^e
020149061	1.2905	$\text{H}\alpha$	$10.18^{+0.23}_{-0.23}$	9.89	$11.29^{+0.80}_{-0.80}$	4.8	3.68 ± 0.08	1.09 ± 0.69	$107 \pm 210^{\text{d}}$	1.5	ROT
020164388	1.3547	$\text{H}\alpha$	$10.13^{+0.31}_{-0.31}$	9.83	$10.77^{+0.26}_{-0.33}$	8.2	2.78 ± 2.27	2.72 ± 0.05	79 ± 19	1.5	NON-R
020167131	1.2246	[OIII] ^c	$10.08^{+0.19}_{-0.19}$	9.81	$9.83^{+0.17}_{-0.10}$	1.8	3.96 ± 0.33	2.60 ± 0.09	127 ± 29	5.0	NON-R
020182331	1.2290	$\text{H}\alpha$	$10.72^{+0.11}_{-0.11}$	9.92	$10.51^{+0.14}_{-0.14}$	5.5	3.49 ± 2.08	4.19 ± 0.17	$127 \pm 25^{\text{d}}$	1.9	NON-R
020193070	1.0279	$\text{H}\alpha$	$10.15^{+0.20}_{-0.20}$	9.57	$10.14^{+0.07}_{-0.07}$	3.9	4.11 ± 1.37	3.49 ± 0.09	$116 \pm 23^{\text{d}}$	3.6	NON-R
020208482	1.0375	$\text{H}\alpha^{\text{c}}$	$10.17^{+0.16}_{-0.16}$	8.94	$9.92^{+0.11}_{-0.08}$	1.4	5.50 ± 0.08	3.67 ± 0.20	158 ± 31	22.9	ROT
020214655	1.0395	$\text{H}\alpha$	$10.02^{+0.16}_{-0.16}$	9.90	$10.91^{+0.31}_{-0.43}$	5.7	3.23 ± 1.05	1.47 ± 0.08	52 ± 14	0.8	NON-R
020217890	1.5129 ^a	$\text{H}\alpha$	$10.02^{+0.16}_{-0.16}$	3.57 ± 0.14
020239133	1.0194	$\text{H}\alpha$	$9.89^{+0.19}_{-0.19}$	9.49	$10.59^{+0.18}_{-0.17}$	4.8	3.09 ± 0.08	3.14 ± 0.09	$148 \pm 33^{\text{d}}$	2.0	ROT
020240675	1.3270	$\text{H}\alpha$	$9.96^{+0.18}_{-0.18}$	9.50	$10.17^{+0.62}_{-0.62}$	3.8	2.85 ± 0.75	1.09 ± 0.16	$47 \pm 92^{\text{d}}$	1.4	NON-R
020255799	1.0351	$\text{H}\alpha^{\text{c}}$	$9.87^{+0.18}_{-0.18}$	9.44	$10.37^{+0.36}_{-0.36}$	4.0	2.91 ± 0.08	1.89 ± 0.26	14 ± 25	0.2	NON-R
020261328	1.5290	$\text{H}\alpha$	$10.01^{+0.26}_{-0.20}$	9.59	$10.65^{+0.34}_{-0.28}$	5.1	3.22 ± 0.08	1.83 ± 0.27	$120 \pm 33^{\text{d}}$	2.2	ROT
020278667	1.0516	$\text{H}\alpha^{\text{c}}$	$10.28^{+0.16}_{-0.16}$	9.04	$9.28^{+0.36}_{-0.36}$	1.3	2.35 ± 0.08	2.82 ± 1.66	$76 \pm 187^{\text{d}}$	1.5	NON-R
020283083	1.2818	$\text{H}\alpha$	$10.05^{+0.21}_{-0.21}$	9.52	$9.89^{+0.23}_{-0.21}$	5.6	2.76 ± 0.16	4.29 ± 0.20	59 ± 12	1.5	NON-R
020283830	1.3949	$\text{H}\alpha$	$10.37^{+0.17}_{-0.17}$	9.94	$10.81^{+0.03}_{-0.01}$	7.9	3.96 ± 0.33	6.82 ± 0.16	186 ± 30	11.3	ROT
020294045	1.0028	$\text{H}\alpha$	$9.80^{+0.15}_{-0.15}$	9.55	$10.93^{+0.21}_{-0.16}$	5.5	3.85 ± 0.16	2.89 ± 0.10	$233 \pm 51^{\text{d}}$	3.9	NON-R
020306817	1.2225 ^a	[OIII]	$9.76^{+0.20}_{-0.20}$	4.22 ± 0.09
020363717	1.3339	$\text{H}\alpha$	$9.68^{+0.35}_{-0.29}$	9.90	$11.89^{+0.28}_{-0.28}$	6.0	3.11 ± 0.08	0.72 ± 0.09	$43 \pm 85^{\text{d}}$	0.5	NON-R
020370467	1.3338	$\text{H}\alpha$	$10.57^{+0.14}_{-0.14}$	10.02	$11.22^{+0.00}_{-0.54}$	5.5	3.53 ± 0.08	1.31 ± 0.25	51 ± 65	0.6	NON-R
020386743	1.0487	$\text{H}\alpha$	$9.88^{+0.20}_{-0.20}$	9.80	$10.21^{+0.25}_{-0.33}$	5.4	2.99 ± 3.32	2.68 ± 0.21	$41 \pm 10^{\text{d}}$	0.8	NON-R
020461235	1.0349	$\text{H}\alpha$	$10.36^{+0.15}_{-0.15}$	9.40	$9.99^{+0.18}_{-0.19}$	5.4	3.47 ± 0.16	3.96 ± 0.12	82 ± 16	3.5	ROT
020461893	1.0486	$\text{H}\alpha$	$9.66^{+0.21}_{-0.21}$	9.54	$10.65^{+0.23}_{-0.31}$	6.5	3.56 ± 0.08	2.66 ± 0.11	58 ± 13	0.9	ROT ^e
020465775	1.3583	$\text{H}\alpha$	$10.12^{+0.20}_{-0.20}$	9.99	$10.25^{+0.21}_{-0.25}$	4.9	3.70 ± 0.08	4.04 ± 0.16	68 ± 15	0.8	NON-R
140083410	0.9435	$\text{H}\alpha$	$10.07^{+0.18}_{-0.18}$	9.78	$10.62^{+0.35}_{-0.35}$	5.3	3.00 ± 0.08	1.93 ± 0.19	30 ± 33	0.4	NON-R
140096645	0.9655	$\text{H}\alpha$	$10.40^{+0.24}_{-0.23}$	10.12	$11.11^{+0.63}_{-0.63}$	4.5	3.41 ± 0.08	1.80 ± 0.40	295 ± 710	3.9	ROT
140123568	1.0012	$\text{H}\alpha^{\text{c}}$	$9.73^{+0.39}_{-0.39}$	9.24	$8.75^{+0.49}_{-0.49}$	0.5	1.44 ± 0.08	1.39 ± 0.98	$50 \pm 97^{\text{d}}$	0.7	NON-R
140137235	1.0445	$\text{H}\alpha^{\text{c}}$	$10.07^{+0.29}_{-0.29}$	9.77	$8.78^{+0.31}_{-0.31}$	0.7	1.54 ± 1.62	5.45 ± 2.03	$61 \pm 11^{\text{d}}$	3.5	ROT
140217425	0.9792	$\text{H}\alpha$	$10.84^{+0.17}_{-0.17}$	10.45	$11.85^{+0.04}_{-0.04}$	14.5	5.50 ± 0.80	8.96 ± 0.13	$320 \pm 46^{\text{d}}$	7.1	ROT
140258511	1.2423	$\text{H}\alpha$	$11.82^{+0.06}_{-0.09}$	10.21	$10.41^{+0.33}_{-0.33}$	5.2	3.17 ± 0.08	2.62 ± 2.11	124 ± 26	5.1	ROT
140262766	1.2836	$\text{H}\alpha$	$9.84^{+0.43}_{-0.43}$	9.38	$10.39^{+0.30}_{-0.30}$	4.1	3.09 ± 0.08	2.07 ± 0.70	$114 \pm 226^{\text{d}}$	3.0	ROT
140545062	1.0408	$\text{H}\alpha$	$10.60^{+0.18}_{-0.18}$	9.61	$11.10^{+0.40}_{-0.40}$	7.5	2.93 ± 0.24	2.89 ± 6.86	$202 \pm 45^{\text{d}}$	3.0	ROT
220014252	1.3105	$\text{H}\alpha$	$10.78^{+0.21}_{-0.21}$	10.42	$11.35^{+0.26}_{-0.26}$	10.3	4.95 ± 0.16	3.32 ± 0.12	129 ± 27	1.4	ROT
220015726	1.2933	$\text{H}\alpha$	$10.77^{+0.27}_{-0.27}$	10.09	$10.72^{+0.20}_{-0.20}$	3.7	2.85 ± 0.08	2.76 ± 0.25	231 ± 354	3.7	ROT
220071601	1.3538 ^{a,b}	$\text{H}\alpha$	$10.81^{+0.59}_{-0.59}$	8.13 ± 0.13
220148046	2.2442 ^b	[OIII] ^c	$11.22^{+0.17}_{-0.17}$	10.10	$8.72^{+0.06}_{-0.06}$	0.9	0.82 ± 0.08	1.98 ± 0.38	61 ± 119	1.3	NON-R
220376206	1.2445	$\text{H}\alpha$	$10.67^{+0.24}_{-0.24}$	10.51	$11.14^{+0.12}_{-0.12}$	10.0	5.42 ± 0.08	5.29 ± 0.08	201 ± 27	2.8	ROT
220386469	1.0226 ^b	$\text{H}\alpha^{\text{c}}$	$10.80^{+0.18}_{-0.18}$	9.64	$9.25^{+0.31}_{-0.32}$	2.6	1.77 ± 0.08	2.90 ± 0.13	$98 \pm 20^{\text{d}}$	2.3	NON-R
220397579	1.0379	$\text{H}\alpha$	$10.23^{+0.19}_{-0.17}$	10.23	$10.97^{+0.23}_{-0.33}$	10.2	3.00 ± 0.07	3.02 ± 0.32	$9 \pm 10^{\text{d}}$	0.2	NON-R
220544103	1.3973	$\text{H}\alpha$	$10.71^{+0.27}_{-0.27}$	10.27	$10.70^{+0.00}_{-0.20}$	7.6	5.31 ± 0.08	5.61 ± 19.8	137 ± 24	1.9	ROT
220544394	1.0101	$\text{H}\alpha$	$10.34^{+0.23}_{-0.23}$	9.97	$9.98^{+0.21}_{-0.21}$	5.0	4.49 ± 0.08	3.40 ± 0.15	55 ± 11	1.1	NON-R
220576226	1.0217	$\text{H}\alpha$	$10.31^{+0.23}_{-0.23}$	9.97	$10.48^{+0.28}_{-0.28}$	6.1	3.22 ± 0.08	2.16 ± 0.12	30 ± 12	0.6	NON-R
220578040	1.0462	$\text{H}\alpha$	$10.72^{+0.17}_{-0.16}$	9.80	$11.05^{+0.41}_{-0.27}$	7.0	6.55 ± 0.08	3.81 ± 0.12	$244 \pm 211^{\text{d}}$	4.9	ROT
220584167	1.4655	$\text{H}\alpha$	$11.21^{+0.24}_{-0.24}$	10.51	$11.28^{+0.07}_{-0.07}$	13.1	5.24 ± 0.08	7.17 ± 0.19	235 ± 35	4.8	ROT
220596913	1.2658 ^b	$\text{H}\alpha$	$10.68^{+0.30}_{-0.30}$	9.53	$10.66^{+0.04}_{-0.04}$	9.3	5.09 ± 0.08	9.49 ± 11.5	141 ± 10	3.7	ROT
910193711	1.5564 ^b	$\text{H}\alpha$	$9.99^{+0.42}_{-0.18}$	10.14	$10.39^{+0.31}_{-0.44}$	4.1	1.61 ± 0.08	2.27 ± 0.06	63 ± 12	0.8	NON-R
910279515	1.4013 ^b	$\text{H}\alpha^{\text{c}}$	$10.79^{+0.14}_{-0.14}$	9.71	$10.34^{+0.07}_{-0.05}$	2.7	4.05 ± 0.25	4.44 ± 0.11	265 ± 18	5.6	ROT

Tab. 2. (1) VVDS identification number. (2) Redshift derived from SINFONI observations of the emission line ($\text{H}\alpha \lambda 6563\text{\AA}$ or [OIII] $\lambda 5007\text{\AA}$) tabulated in column (3). (4) Stellar mass in solar mass units. (5) Gas mass derived using the Kennicutt-Schmidt formulation (Kennicutt 1998b). (6) Dynamical mass computed following Eq. 1 and based on the best-fitting parameters of the kinematic model. (7) The radius computed as the total size of the ionized emission map with a confidence level larger than 2σ . (8) The gas half-light radius estimated on the SINFONI maps of the lines tabulated in column (3). (9) The observed I-band half-light radius. (10) Maximum velocity deduced from model fitting. (11) Ratio of the maximum rotation velocity over the velocity dispersion. (12) Kinematic classification (R: Rotating objects, NON-R: non-rotating systems). ^a This redshift is computed on the original VIMOS spectrum. ^b Observations with Adaptive Optics. ^c Galaxy with low signal-to-noise ratio ($3 \leq S/N \leq 4.5$) plotted with empty symbols in the figures. Galactic properties of SINFONI observations with a signal-to-noise ratio below 3 are not reported. ^d Galaxy for which the plateau velocity has not been reached. ^e Galaxy for which the criterion on $v/\sigma > 1$ is not fulfilled, thus not included in the purely rotating disc sample. The public access to data is at <http://cosmosdb.iasf-milano.inaf.it/VVDS-SINFONI>.

The SFRs were computed following Kennicutt (1998a). The fluxes were measured in $> 2\sigma$ regions of the flux-calibrated data cubes and corrected for dust reddening using the extinction coefficient derived from the SED fitting (see Contini et al. 2012). The half-light radius, $R_{1/2,gas}$, was measured with GALFIT (Peng et al. 2002) as the semi-major-axis half-light radius describing the spatial extent of the ionized gas ($\text{H}\alpha\lambda6563\text{\AA}$ or $[\text{OIII}]\lambda5007\text{\AA}$) emission, after convolving the images with the PSF of a bright star nearest in time to the scientific observations. Maps of the residuals were used to optimize the results. Assuming that the Schmidt law holds in our redshift interval, we estimated the gas mass M_{gas} using the relation between the gas density Σ_{gas} and the star-formation rate surface density Σ_{SFR} (Kennicutt 1998b)

$$\frac{\Sigma_{\text{SFR}}}{\text{M}_\odot \text{ yr}^{-1} \text{ kpc}^{-2}} = 2.5 \times 10^{-4} \left(\frac{\Sigma_{\text{gas}}}{\text{M}_\odot \text{ pc}^{-2}} \right)^{1.4}, \quad (2)$$

where the relation between the observed $\text{H}\alpha$ luminosity per unit area, or the $\text{H}\alpha$ surface density $\Sigma_{\text{H}\alpha}$, and the gas surface density is

$$\frac{\Sigma_{\text{gas}}}{\text{M}_\odot \text{ pc}^{-2}} = 1.6 \times 10^{-27} \left(\frac{\Sigma_{\text{H}\alpha}}{\text{erg s}^{-1} \text{ kpc}^{-2}} \right)^{0.71}. \quad (3)$$

The mass of the gas associated with the measured star formation is given by

$$M_{\text{gas}} = \Sigma_{\text{gas}} \times \text{Area}, \quad (4)$$

where the *Area* in Eq. 4 is the total spatial extent of the ionized gas measured in $> 2\sigma$ regions of the flux-calibrated data cubes.

The gaseous masses are given in Tab. 2, and their associated error was analytically propagated from the errors in the observations using conventional techniques. Further details of the error analysis are described in Epinat et al. (2012). Typical value of the error is of the order of 0.25 dex. We note that different calibrations exist for the Kennicutt-Schmidt law at higher redshift, e.g., Bouché et al. (2007) suggest a steeper power-law index (1.7 instead of 1.4 in Eq. 3) for $z > 2.5$ starburst galaxies. This steeper formulation implies a < 0.3 dex difference in the gas computation. Given the uncertainties involved in deriving this quantity, a different value for the slope does not have any significant impact on our data interpretations (see Gnerucci et al. 2011).

3.3. Kinematic classification

To classify our sample, we adopt a kinematic classification that relies on a combination of observed galaxy properties. We refer to Epinat et al. (2012) for a full description of the methodology of which we provide here a brief outline. In a first step, eight of us classified independently all the sample using personal criteria. Subsequently, we reconciled the criteria into a newly agreed scheme: we assigned to each galaxy a confidence flag generated by the concordance among the classifiers.

When galaxies satisfy all the following conditions, they are kinematically flagged either as:

Rotating discs: when the velocity field is well described by a symmetrically rotating disc with a kinematic position angle that does not differ significantly from the morphologically derived major axis. We quantify these conditions assuming that the mismatch between the position angles is smaller than $\pm 20^\circ$ and that the residuals of the modelled velocity field

over the measured velocities are less than a certain fraction ($< 20\%$). In this work, galaxies are classified as “rotators” when they are rotationally supported such that their rotation velocity is larger than their dispersion velocity (i.e., $v/\sigma > 1$ as listed in column (12) of Tab. 2),

or

Non-rotating systems: At least one of the conditions about the residuals, position angles, or rotation-over-chaotic motions is violated. This class includes galaxies with some kind of anomalies in their velocity field, merger-like systems, and/or objects with off-peak distributions of the dispersion velocity, but also possibly slow rotators or face-on systems with an observed velocity gradient smaller than typically $\pm 25 \text{ km s}^{-1}$.

4. The gas properties in MASSIV star-forming galaxies

We compare the total extent of the ionized gas, R_{last} , with the half-light radius of the stellar component, $R_{1/2,\text{star}}$, for the class of rotating and non-rotating disc galaxies in Fig. 1 (in the top panel with blue colour-coded circles and in the bottom panel with red colour-coded squares, respectively). The radius R_{last} is computed as the total size of the ionized emission map that has a confidence level larger than 2σ . The half-light radius of stars is measured on the observed I-band images, or at rest-frame U-band wavelengths. The error bars in Fig. 1 are the 1σ uncertainties derived from the GALFIT procedure on the images corrected for their respective PSF FWHM. The histograms show the distributions of the gas and stellar radii of the classes. The solid line is the linear fit² to the data and the dashed line shows the standard deviation.

The dotted line is the correlation observed in a thin exponential disc between the radius of the total ionized gas emission and the half-light radius of the stellar component, $R_{\text{last}} \sim 1.9 \times R_{1/2,\text{star}}$. Assuming that the optical radius equals 3.2 times the disc scalelength following Persic & Salucci (1991), the half-light radius is 1.678 times the disc scale length. The total ionized gas, R_{last} , is close to the optical radius measured for local star-forming galaxies (e.g., Garrido et al. 2005).

For the class of rotators, we obtained median values of $R_{\text{last}} = 5.40_{-4.80}^{+7.60} \text{ kpc}$ and $R_{1/2,\text{star}} = 3.51_{-2.62}^{+5.29} \text{ kpc}$, and for non-rotators $R_{\text{last}} = 5.50_{-4.00}^{+6.50} \text{ kpc}$ and $R_{1/2,\text{star}} = 2.68_{-1.47}^{+3.40} \text{ kpc}$ (with the extremes representing the quartiles of the distribution for the two classes). Non-rotating galaxies were found to have more compact stellar components than rotators, but similarly sized gas components. For rotating galaxies, we found that $R_{\text{last}} = 1.63 \pm 0.14 \times R_{1/2,\text{star}}$ with an intrinsic scatter of $\sigma_{\text{intr}} = 2.23$ (and total scatter of $\sigma_{\text{tot}} = 2.70$). The same correlation for non-rotating systems is $R_{\text{last}} = 1.70 \pm 0.21 \times R_{1/2,\text{star}}$ ($\sigma_{\text{intr}} = 2.20$ and $\sigma_{\text{tot}} = 2.66$). In the local Universe, the size of the ionized gas component of star-forming galaxies is close to the optical radius (e.g., Garrido et al. 2005). Within 1σ dispersion, and considering the associated uncertainties, all MASSIV rotating galaxies are within the expected statistical trend found by Persic & Salucci (1991). A similar agreement was found by Puech et al. (2010) for

² We fit a linear relationship to the data using the MPFITEXY routines (Williams et al. 2010). The MPFITEXY routine depends on the MPFIT package (Markwardt 2009). This routine properly adjusts the intrinsic scatter to ensure the minimisation of chi-square with an iterative prescription.

their IMAGES sample at $z \sim 0.6$. As for Puech et al. (2010) and Bamford et al. (2007), we note that the fraction of non-rotating galaxies with a larger gaseous extent than their stellar counterpart exceeds the predicted correlation by 1σ . While in the sample of Puech et al. (2010) the cases where this correlation is not respected are the ones with the UV light extending further out the field-of-view of the FLAMES/IFU ($3'' \times 2''$), in the MASSIV sample the two outliers show a signature of a close companion, one of which is detected in H α .

We will investigate these trends and their relation to the environment at the completion of the survey when we will develop a classification scheme enabling us to distinguish the various mechanisms of disturbance in inclined and face-on galaxies as well as in compact and dispersion-dominated spheroids. For simplicity, at the present time we flag all these galaxies in a unique class named non-rotators (plotted with red-coded, square symbols in all figures).

We now compare our measurements with the characteristic sizes of galaxies measured by other similar surveys to analyse the correlation among properties such as stellar mass, size, and velocity. In IMAGES (Puech et al. 2010), the total light radius measured in observations of the ionized [OII] gas of rotating galaxies has a median of 11.29 kpc and ranges from 8.25 kpc (first quartile, or 25th percentile of distribution) to 11.99 kpc (last quartile, or 75th percentile). The median value of the half-light rest-frame UV radius is 6.27 kpc where 4.26 kpc and 6.53 kpc are quartiles of the distribution. We note that the IMAGES disc size reaches a maximum between the total size measured in the ionized [OII] gas and the half-light rest-frame UV light multiplied by 1.9. In SINS (Cresci et al. 2009), the half-width half-maximum size (HWHM) measured on the ionized H α maps by Bouché et al. (2007) is interpreted as the exponential disc scale-lengths of $z \sim 2$ rotating SINS discs, and ranges from 4.11 kpc to 6.35 kpc with a median of 5.87 kpc. The circular half-light sizes of the total SINS $z > 2$ sample computed on H α maps by Förster Schreiber et al. (2009) is in the range 2.40 – 4.60 kpc and has a median value of 3.10 kpc. Dutton et al. (2011) claim that there is a fundamental disagreement between the SINS HWHM sizes published in Cresci et al. (2009) and the SINS half-light radii measured by Förster Schreiber et al. (2009), as already noted by these latter authors who reject the possibility that this discrepancy is caused by non-exponential discs. At higher redshift, the AMAZE/LSD sample of Gnerucci et al. (2011) is constituted of eleven $z \sim 3$ rotating galaxies. The characteristic radius of these exponential discs measured in H α maps ranges between 0.71 kpc and 1.73 kpc (first and last quartile of the distribution) with a median value of 1.24 kpc. Comparing directly to the values of Puech et al. (2010) since we adopt the same radius definition, we find overall that IMAGES radii are a factor of 1.5 larger than our MASSIV radii. When comparing with the radii derived for SINS by Förster Schreiber et al. (2009), we find similar sizes (our half-light sizes measured in our H α maps being in the interval $R_{1/2,gas} = 2.85 - 3.96$ kpc with a median of 3.47 kpc). Both SINS and MASSIV radii are approximately three times larger than sizes sampled at $z \sim 3$ in AMAZE/LSD by Gnerucci et al. (2011).

We investigate the disc properties to verify the hypothesis of whether our MASSIV discs have exponential profiles. Discs of ionized gas frequently have an irregular, clumpy distribution, as previously reported for SINS galaxies. Despite the simplistic assumptions, both a Sérsic index distribution and a correlation between exponential and half-light radii suggest that MASSIV discs can be approximated as exponential discs. The same qualitative

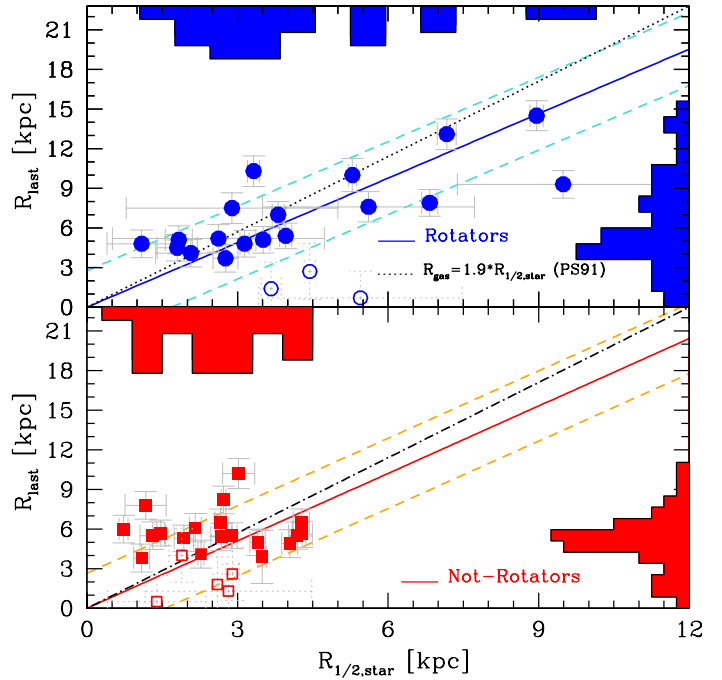


Fig. 1. Comparison between R_{last} and $R_{1/2,star}$ radii computed as the size of our ionized gas maps with a confidence level larger than 2σ and the half-light radius of the stellar continuum measured on the observed I-band best-seeing CFHTLS images, respectively. Within the errors, both rotators (top panel, blue circle) and non-rotators (bottom panel, red square) agree with the expected statistical trend $R_{last} = 1.9 \times R_{1/2,star}$ found by Persic & Salucci (1991, PS91) plotted with a black dotted line. The blue/red solid lines are the best-fit relation found for the rotators/non-rotating galaxies (dashed lines show the total scatter of the correlations). The empty symbols show galaxies detected with a low S/N ($3 \leq S/N \leq 4.5$).

conclusion was reported for SINS discs (Förster Schreiber et al. 2009).

In summary, our resulting characteristic size agrees within the statistical correlations previously assessed in the literature. The radius taken to derive the velocity is critical to avoid the introduction of systematic biases (see Noordermeer & Verheijen 2007). The relation obtained between the size of the stars and that of the gaseous component ensures that this latter physical quantity is reliable for the determination of the maximum velocity.

Figure 2 shows the stellar mass of MASSIV galaxies versus the dynamical (top panel) and gas (bottom panel) mass. The methods used to derive these masses are described in Sect. 3.2. The total distributions of these quantities are shown as full grey-coded histograms, while those with blue, positive-oblique angle (or red negative-oblique angle symbols) refer to rotating (non-rotating) galaxies. Dynamical masses range between $2.57 \times 10^{10} M_{\odot}$ and $1.29 \times 10^{11} M_{\odot}$ with a median value of $5.01 \times 10^{10} M_{\odot}$ for the class of rotating galaxies (dashed-point horizontal line in the bottom panel of Fig. 2), and $0.95 - 8.13 \times 10^{10} M_{\odot}$ with a median value of $2.45 \times 10^{10} M_{\odot}$ for non-rotating galaxies (dashed horizontal line). We estimated a gaseous mass in the interval between $3.38 \times 10^9 M_{\odot}$ (first quartile) and $1.64 \times 10^{10} M_{\odot}$ (last quartile) with a median value of $7.85 \times 10^9 M_{\odot}$, and stellar

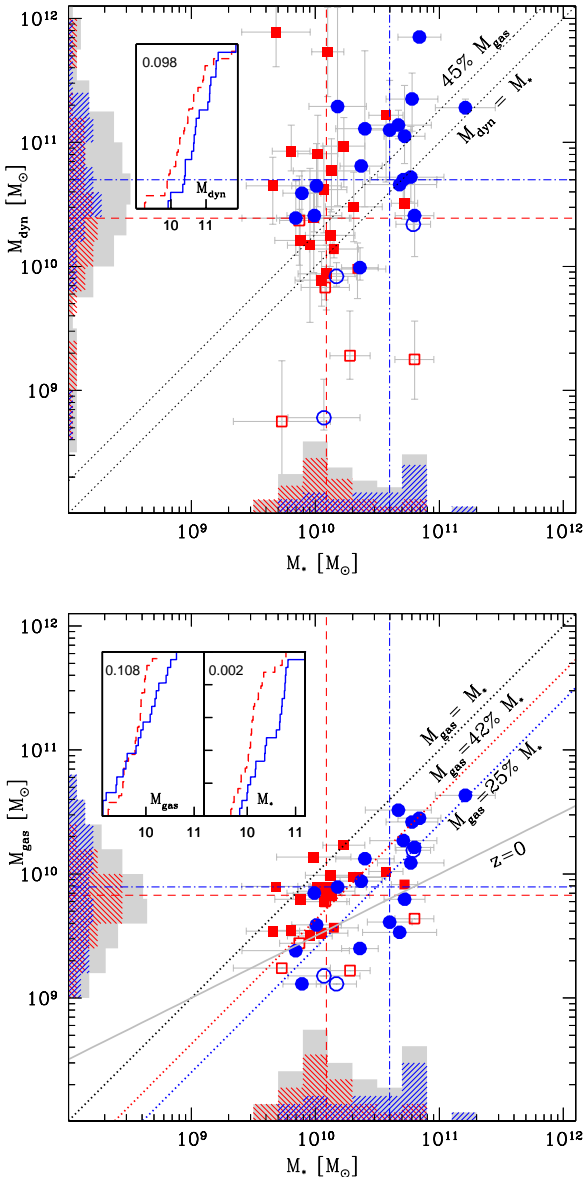


Fig. 2. The stellar mass content of MASSIV galaxies compared to both the dynamical mass derived from the dynamical modelling (top panel) and gas content derived using the Kennicutt-Schmidt formulation (bottom panel). Symbols are as in Fig. 1. The horizontal and vertical histograms represent the distribution of the stellar and dynamical masses (top) and gas mass (bottom panel). The horizontal and vertical lines are the median values of rotators (point-dashed blue line) and non-rotators (dashed red line), respectively. Dashed diagonal lines in the bottom panel comply with the condition $M_{\text{gas}} = \text{frac} \times M_{\text{star}}$, where frac is equal to 25% for rotating galaxies and 42% for non-rotators (or 20% and 30% of the baryonic mass, respectively). The solid line is the local relation proposed by Schiminovich (2008) using the GALEX Arecibo SDSS survey of cold HI gas. In the inserted panels, the cumulative distributions for stellar-, dynamical-, and gas-mass are plotted for rotators (solid, blue line) and non-rotators (dashed, red line) along with the probability for the two classes to be statistically different.

masses in the range $1.48 - 5.87 \times 10^{10} M_{\odot}$ with a median value of $3.98 \times 10^{10} M_{\odot}$ in rotating galaxies. Median values for non-rotators are $M_{\text{star}} = 1.23 \times 10^{10} M_{\odot}$ and $M_{\text{gas}} = 6.71 \times 10^9 M_{\odot}$ with ranges between $\Delta M_{\text{star}} = 0.90 - 1.90 \times 10^{10} M_{\odot}$ and $\Delta M_{\text{gas}} = 3.51 - 9.37 \times 10^9 M_{\odot}$.

Within their uncertainties, only a few galaxies lie in the forbidden region of $M_{\text{star}} > M_{\text{dyn}}$. The only strongly deviating rotating galaxy (empty, dashed symbol) was detected with a low S/N (~ 3.5). We inferred a probability of $P = 7.5 \times 10^{-2}$ and $P = 1.5 \times 10^{-4}$ that the stellar mass is uncorrelated to both the dynamical and gas mass using the Spearman correlation test. The correlation is statistically significant in particular for the stellar and gas masses. In the insert panels of Fig. 2, we show the cumulative distributions of these quantities for rotators (solid, blue line) and non-rotators (dashed, red line), along with the probability that the two classes are statistically different based on the Kolmogorov-Smirnov test.

We assume no contribution from dark matter in the inner regions of galaxies. This is the most likely hypothesis given our inability to measure the dark matter distribution in high- z galaxies. This hypothesis was adopted in earlier studies, e.g., by Gnerucci et al. (2011). With this assumption, the mass in gas taken as the difference between the dynamical and stellar masses of both classes of rotator and non-rotator galaxies, is on average a fraction of $\sim 45\%$ of the dynamical mass (diagonal dotted line), and approximately either 20% of the stellar mass or 17% of the baryonic mass. A consistency picture is obtained for rotating galaxies when deriving the gas mass from the Kennicutt-Schmidt law. We found that the gas mass is 25% of the stellar mass (or 20% of the baryonic mass) in rotating galaxies with typical errors associated with the fit of the order of 5 – 6%.

The gas content in non-rotating galaxies is definitively higher ($\sim 42\%$ of the stellar mass, or 30% of the baryonic mass) when using the Kennicutt-Schmidt law. Taking into account that this class of galaxies may contain face-on discs, this fraction represents a lower limit. The same value derived as a difference between dynamical and stellar mass is somehow lower. It can be justified by two factors: 1) the inclusion of merging systems in the class of non-rotating galaxies that may have not yet exhausted their gas reservoir; 2) the different properties of dark matter halos in rotators and spheroidal galaxies. In nearby galaxies, within the optical radius the dark matter content is suspected to be higher in rotators than in spheroids (Persic et al. 1996). Thus, for the same dynamical mass, the fraction of gas and stars should be lower in rotators than in our class of non-rotating systems.

If we fix the slope to the local relation proposed by Schiminovich (2008) using the GALEX Arecibo SDSS survey of cold HI gas, we obtain a weak evolution of +0.17 dex to $z = 1.2$ for the entire sample (or +0.11 dex for rotators and +0.21 dex for non-rotating galaxies). We emphasize that the selection criteria adopted to build up the MASSIV sample lead to a subsample of non-rotating galaxies with a lower content of stellar mass at fixed gas and dynamical mass.

The fraction of gas in $z \sim 0.6$ IMAGES galaxies ranges between 30% as derived from the evolution of the gas-metallicity relation (Rodrigues et al. 2008) and 45% of the stellar mass obtained with the inverse Kennicutt-Schmidt law by Puech et al. (2010). The gas fraction quoted by Cresci et al. (2009) for SINS galaxies at $z \sim 2$ is in the interval 23 – 30% of the dynamical mass, but including a dark matter contribution of 40%. At higher redshift ($z > 3$, the AMAZE/LSD surveys), these values are too uncertain (Gnerucci et al. 2011).

On the basis of direct estimates using molecular observations (e.g., Daddi et al. 2010; Tacconi et al. 2010), the gas mass in disc galaxies has been found to be 34–44% of the baryonic mass, and have slowly decreased in the past 8–10 Gyr. Our results are in full agreement with a slow decrease in the gas mass content in disc galaxies since $z \sim 1.2$ with a gas fraction that then halves progressively prior to the redshift of the local Universe.

5. The size - mass - velocity relation

We now examine the fundamental relations existing in the MASSIV sample at $1.0 < z < 1.6$. We compare their sizes, stellar masses, and rotation velocities to galaxy samples available in the literature at different redshifts to investigate the evolution of these properties. In particular, we derive the relation between the luminosity (or stellar mass) and rotational velocity introduced by Tully & Fisher (1977), the so-called Tully-Fisher relation (TFR). We explore the shift in the zero point of this relation and the other fundamental relations that unveil the inter-connection between dark and luminous matter for galaxies at different cosmic epochs.

5.1. The size - mass relation

The evolution of the size - stellar mass relation in rotating galaxies at $1.0 < z < 1.6$ is shown in the top panel of Fig. 3. The distribution of the MASSIV rotating galaxies in this plot (blue-coded circles) is consistent with a mild dependence of the disc size on the stellar mass. Taking into account the relatively limited statistics associated to a disc size representing only a lower limit (as measured for galaxies with a S/N above 3), we interpret this plot in the framework of its evolution with respect to the local relation by fixing the slope to the local relation as derived by Dutton et al. (2011). This relation is based on the local I-band disc scalelength - stellar mass relation of Dutton et al. (2007) with stellar masses from Bell et al. (2003) and Bell & de Jong (2001). The evolution of the relation is only slightly stronger using the V-band instead of the I-band size-stellar mass relation derived from the SDSS data. This radius is scaled to the half-light radius, which is 1.678 times the scale length for the exponential profile. This local relation is plotted in Fig. 3 as a dashed, black line. The solid, blue line is the fit to the MASSIV rotating galaxies. To make a consistent comparison to our measurements, we plot in this figure only the evolution reported in those studies using the sizes measured in the ionized gas ($\text{H}\alpha$, or $[\text{OII}]$) maps. The best fit obtained using SINS galactic sizes defined as the HWHM $\text{H}\alpha$ radii (Bouché et al. 2007; Cresci et al. 2009) is plotted with a dotted-dashed, orange line and a long-dashed, orange line when the size is defined as the half-light $\text{H}\alpha$ radius by Förster Schreiber et al. (2009). We note that the difference in the evolution of this relation is due to the method used to measure the disc sizes by Bouché et al. (2007) and Förster Schreiber et al. (2009) (cf. Dutton et al. 2011). We plot with a dotted, red line the evolution measured for IMAGES rotating galaxies using as disc size the maximum between the total size measured about the ionized $[\text{OII}]$ gas and the half-light rest-frame UV light multiplied by 1.9. All quantities are consistently rescaled to our Salpeter IMF.

There is a general consensus about the mild evolution of the disc size in star-forming galaxies up to $z \sim 1$ (for example as measured by Williams et al. (2010) taking the circularized rest-frame I-band half-light radii of disc-dominated galaxies, and by Trujillo et al. (2006) taking the circularized

rest-frame V-band half-light radius). Compared to the present-day disc sizes, the $z = 1$ counterparts are *smaller* by ~ 0.10 dex at fixed stellar mass and rotation velocity (e.g., Dutton et al. 2011). This picture agrees well with the theoretical predictions (Blumenthal et al. 1984; Dalcanton et al. 1997; Mo et al. 1998; Firmani & Avila-Reese 2000; de Jong & Lacey 2000; Pizagno et al. 2005; Dutton et al. 2007).

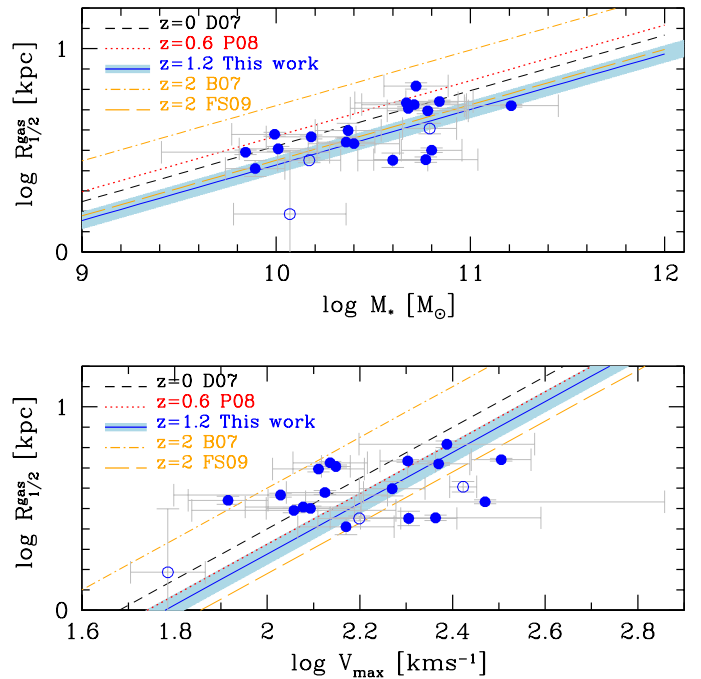


Fig. 3. The stellar mass-size relation (**top panel**) and the velocity-size relation (**bottom panel**) for MASSIV rotating galaxies at $z \sim 1.2$ (solid, blue line with the 1σ error of the correlation illustrated by the light blue area). The local relation of Dutton et al. (2007, D07) is shown as a short-dashed, black line. We overplot the best-fit relations obtained by Puech et al. (2008) (P08, $z \sim 0.6$, dotted red line), Bouché et al. (2007), and Cresci et al. (2009) at $z \sim 2$ (B07, dotted-dashed orange line), and Dutton et al. (2011) using measurements of Förster Schreiber et al. (2009) (FS09, $z \sim 2$, long-dashed orange line). The symbols are as in Fig. 1.

At $z \sim 1.2$, we report an evolution size–stellar mass relation of -0.14 dex using the half-light $\text{H}\alpha$ radius, that is quite similar to earlier findings at $z \sim 1$. Above $z \sim 1$, the evolution of disc sizes in the literature is less clear, even with opposite trends. Trujillo et al. (2006) found a factor of two smaller half-light sizes at $z \simeq 2.5$ at fixed stellar mass relative to $z = 0$ galaxies. A similar evolution is reported by Williams et al. (2010) in star-forming galaxies at $z = 2$. The evolution of circular half-light $\text{H}\alpha$ sizes measured by Förster Schreiber et al. (2009) and reported by Dutton et al. (2011) for SINS data at similar redshifts is smaller than previously quoted results, i.e., -0.07 ± 0.05 dex to be compared with -0.28 dex by Trujillo et al. (2006). This discrepancy is attributed by Dutton et al. (2011) to the difference in the half-light radius measured on the $\text{H}\alpha$ maps and rest-frame optical band images. Taking into account this difference, their results can be reconciled. A different trend is obtained using measurements published in Cresci et al. (2009) for the same SINS data

by Dutton et al. (2011). Using the half-width half-maximum size interpreted as exponential disc scale-lengths, SINS disc galaxies presented in Cresci et al. (2009) are ~ 1.6 times *larger* at $z = 2$ than their local counterparts at fixed stellar mass. Even if a factor of -0.07 dex caused by the skewed distribution towards low inclinations reduces the discrepancy, the values remain significantly inconsistent by a factor of three with the measurements of Trujillo et al. (2006) and Williams et al. (2010) (cf. Dutton et al. 2011). This discrepancy between data-sets increases at higher redshifts if we explore the AMAZE/LSD sample by Gnerucci et al. (2011). The sizes of the discs are more than four times *larger* in the past than in their local counterparts. We can cautiously speculate that this strong evolution may be caused by a selection effect in the AMAZE/LSD galaxies and the difficulties in measuring realistically the $\text{H}\alpha$ sizes at such high redshifts ($z \sim 3$).

Comparing the evolution computed directly from the half-light radii measured in $\text{H}\alpha$, we found at $z \sim 1.2$ a similar evolution similar to that derived from SINS data at $z \sim 2$ by Dutton et al. (2011), based on measurements by Förster Schreiber et al. (2009). However, if we account for the shift suggested by Dutton et al. (2011) that converts our $\text{H}\alpha$ sizes at $z \sim 1.2$ to their optical band half-light radii, we should have a stronger evolution with redshift, i.e., -0.21 dex instead of -0.09 ± 0.04 . Conversely, we did not find a conversion similar to that suggested by Dutton et al. (2011) in the ratio of galaxy sizes (e.g., of our observed I-band to $\text{H}\alpha$). Furthermore, our results for the evolution of the disc size perfectly agree with the evolution up to $z \sim 1$ found by Williams et al. (2010) and Trujillo et al. (2006), especially taking into account the associated uncertainties in the measurements and the adopted assumptions. Therefore, on the basis of the current data-set we suggest that there is a mild evolution in the size - stellar mass relation of rotating galaxies at $z \sim 1.2$. A homogeneous comparison of MASSIV galaxies at $z \sim 2$ and $z \sim 1$ that will be possible at the completion of this survey, will provide a definitive answer to this controversial issue.

5.2. The size - velocity relation

The bottom panel of Fig. 3 shows the relation between the disc scale length and the maximum rotation velocity for both MASSIV rotating galaxies and samples from the literature at different redshifts.

The distribution of the MASSIV rotators in this plot (blue-coded circles) is consistent with there being no dependence between the disc size and the stellar mass. For the reasons explained in Sect. 5.1, we discuss hereafter the size-velocity relation using the slope determined for local galaxies. We observe a shift of -0.12 ± 0.05 dex in the relation at $z \sim 1.2$ with respect to the local I-band size-velocity distribution computed by Dutton et al. (2007). As reported by Puech et al. (2007), different calibrations proposed to describe this correlation show very similar results, despite the different quantities used to trace the galactic properties. Puech et al. (2007) found some IMAGES rotating galaxies at $z \sim 0.6$ with a relatively lower disc scale length at fixed velocity than local rotators (cf. blue circles in their Fig. 3), although the majority of the galaxies lies on the distribution of local rotating discs. We fitted their rotating galaxies with a relation showing a marginal evolution of -0.08 ± 0.06 from $z \sim 0.6$ to $z \sim 0$.

At $z \sim 2$, the results differ between authors. A systematic agreement with our measurements is observed at higher redshift when adopting the half-light sizes computed by Förster Schreiber et al. (2009). The evolution at $z \sim 2$ shows even smaller sizes at a given maximum rotation velocity than

lower redshift galaxies with an offset of -0.22 ± 0.06 dex from $z = 2$ to $z = 0$ (cf. Dutton et al. 2011), and -0.10 dex to $z \sim 1.2$. At $z \sim 2$, a different trend is observed by Bouché et al. (2007) combining data from the SINS survey and Courteau (1997) at $z = 0$. Bouché et al. (2007) found no evolution in the zero-point of the size-velocity relation from $z = 2$ to $z = 0$. Dutton et al. (2011) attributed this discrepant result to an inconsistency in the SINS half-width half-maximum size reported in Cresci et al. (2009) and interpreted as exponential disc scale-lengths.

The size-velocity relation shows at all cosmic times a large scatter (of the order of ~ 0.2 dex). The scatter reported in previous analyses at high- z are likely due to the difficulties in discerning kinematically complex systems, which translate into uncertainties in the estimation of the characteristic radius of the system. While we are not unaffected by these uncertainties, the statistical trend observed between the size of our ionized emission maps and our radius of the stellar continuum in the broadband images of rotating galaxies, ensures that we are able to derive reliable quantities. The local relations studied by e.g., Courteau (1997) and Mathewson et al. (1992) and more tightly constrained in this respect, also show a large scatter in this relation suggesting a physical meaning of this dispersion.

5.3. The mass - velocity relation

In the top panel of Fig. 4, we show the correlation between the stellar mass and the rotation velocity at $z \sim 1.2$ of the MASSIV galaxies. Rotating galaxies are plotted with blue-coded circles. They are the sole class of galaxies included in our best-fit procedure. We plot non-rotating galaxies with red-coded, square symbols. The errors in the velocities are computed using simulations in a local sample to account for various uncertainties (see for details Epinat et al. 2008). The errors on the stellar mass are described in Contini et al. (2012). As we did in the previous section, given the relatively limited size of our data set at this stage of the survey we fixed the slope to that of the local calibration. To make a fair comparison with the published data at different redshifts, and to allow for future comparisons, we fitted our data with the two most widely used calibrations. In particular, we calibrated the stellar mass TF relation (smTFR) with the local slope by Pizagno et al. (2007) to compare with the IMAGES sample at $z \sim 0.6$ by Puech et al. (2008, 2010). The local calibration by Pizagno et al. (2007) based on a representative galaxy sub-sample extracted from the SDSS and revised by Hammer et al. (2007) is plotted in Fig. 4 with dashed, black line. The best-fit relation of Puech et al. (2008) is plotted with a dotted red line. We calibrated the relation with the local slope defined by Bell & de Jong (2001) to compare with the SINS sample at $z \sim 2.2$ by Cresci et al. (2009) and with the LSD/AMAZE galaxies at $z \sim 3$ by Gnerucci et al. (2011). The local calibration of Bell & de Jong (2001) is plotted in Fig. 4 with a solid, black line. The best fit by Cresci et al. (2009) is shown with a short-dashed-dotted orange line and that by Gnerucci et al. (2011) with a long-dashed-dotted magenta line. The Bell & de Jong (2001) calibration is based on the local sample of Verheijen (2001), who selected predominantly low-mass, gas-rich galaxies observed with the 21cm HI emission (Puech et al. 2010; Hammer et al. 2007). The resulting relation is steeper than the Pizagno et al. (2007) reference. The two relations are almost equivalent around a velocity of $\sim 200 \text{ km s}^{-1}$ and a stellar mass of $\sim 10^{11} M_\odot$, thus samples with these galactic properties are not substantially affected by the choice of the calibration. The vast majority of our MASSIV galaxies are located below these values. In consequence, adopting one, or the other calibration affects the strength

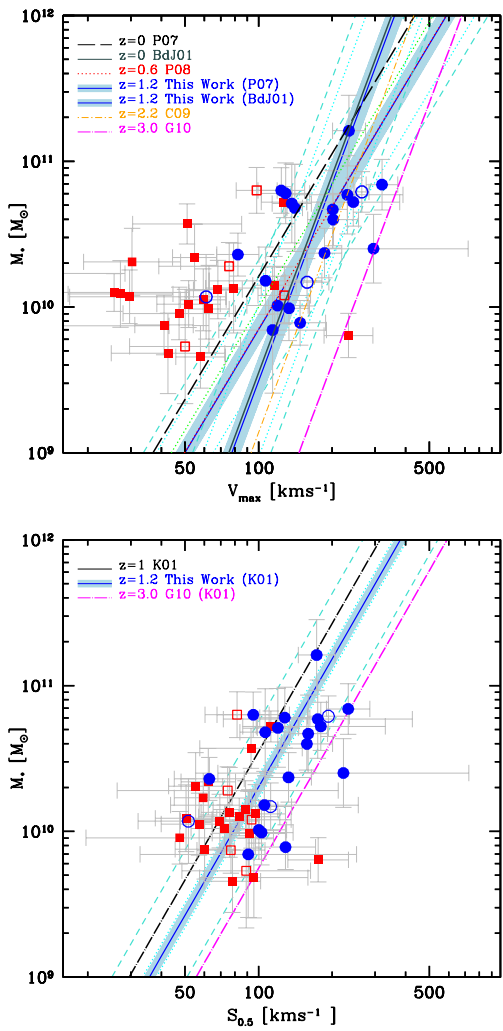


Fig. 4. (Top) The stellar mass TF (smTF) relation at $z \sim 1.2$ based on the MASSIV rotating galaxies. Symbols are as in Fig. 1. Errors in the velocities are computed using GHASP simulations to account for various uncertainties. The smTF for the MASSIV rotators is calibrated using the local slope defined by either Pizagno et al. (2007, P07) or Bell & de Jong (2001, BdJ01) (dashed black line and solid black line, respectively). The solid-blue lines are the best-fit to MASSIV rotating galaxies and the cyan shaded area shows the 1σ error in the zero-point parameter (the intrinsic and total scatter is plotted as cyan dotted line and cyan dashed line, respectively). Other fits are those of Puech et al. (2008) (P08, $z \sim 0.6$, dotted red line), Cresci et al. (2009) (C09, $z \sim 2.2$, short-dashed-dotted orange line), and Gnerucci et al. (2011) (G11, $z \sim 3$, long-dashed-dotted magenta line). **(Bottom)** The relation between the stellar mass and the contribution of both ordered and chaotic motions ($S_{0.5} = \sqrt{0.5 \times v_{rot}^2 + \sigma_0^2}$, Kassin et al. 2001, K01) is shown. The cyan shaded area shows the 1σ error on the zero-point parameter, the cyan dotted line and cyan dashed line are the intrinsic and total scatter, respectively. We overplot the best-fit relation of Kassin et al. (2007) at $z \sim 1$ (K01, dot-dashed black line) and Gnerucci et al. (2011) at $z \sim 3$ (G11, dot-dashed magenta line). Symbols are as in Fig. 1.

of the evolution in the velocity-mass relation. For each calibration, we computed the zero-point of the correlation, its error, its

intrinsic, and total scatter. All the above-mentioned studies have been opportunely rescaled to account for our Salpeter IMF.

For rotators, we obtain an evolution from $z = 0$ in stellar mass of the smTFR zero point of -0.36 ± 0.11 dex, using as reference the SDSS subsample by Pizagno et al. (2007) (with an intrinsic scatter of $\sigma_{intr} = 0.32$ dex and a total scatter of $\sigma_{tot} = 0.48$ dex). Using the Bell & de Jong (2001) calibration, we instead obtain a zero-point at $z \sim 1.2$ that is consistent with no evolution since $z \sim 0$ (or -0.05 ± 0.16 dex, $\sigma_{intr} = 0.52$ and $\sigma_{tot} = 0.72$). The solid, blue lines are the best-fit relation to MASSIV rotators and the cyan shaded area shows the 1σ error on the zero-point parameter (the intrinsic and total scatter is plotted as cyan dotted and cyan dashed line, respectively).

The shift in the zero point of the smTFR with respect to $z = 0$ computed by Puech et al. (2008, 2010) at $z \sim 0.6$ is surprisingly high (-0.34 dex in stellar mass) relative to our results at $z \sim 1.2$. The evolution in the smTFR computed using IMAGES dataset is very similar (within the errors) to the evolution we report at higher redshift (-0.36 ± 0.11 dex at $z \sim 1.2$). There are important issues to be taken into account when interpreting these values. The original evolution claimed by Flores et al. (2006) for the same data-set was consistent with no or marginal evolution. Other authors, using traditional slit spectroscopy, reached the same qualitative conclusion of no/mild evolution up to redshift $z \simeq 1$ (e.g., Weiner et al. 2006; Conselice et al. 2005; Fernández Lorenzo et al. 2010). The IMAGES galaxies have large seeing and coarse spatial resolution owing to the characteristics of the FLAMES instrument (Puech et al. 2010). Furthermore, the lack of evolution in the *baryonic* (star+gas) Tully-Fisher relation reported by Puech et al. (2010) using the same IMAGES sample and a gas fraction at $z \sim 0.6$ that is similar to the values of nearby galaxies, implying that there has been a minimal, if not negligible evolution of the stellar-mass TFR (Dutton et al. 2011). All these points therefore suggest an overestimation of the evolution of the stellar Tully-Fisher relation by Puech et al. (2008) and an evolution of the smTF relation of IMAGES data of the order of -0.1 dex only, instead of the estimated -0.34 dex (Dutton et al. 2011).

If we compare our best fit with the Bell & de Jong (2001) calibration at $z \sim 1.2$ for the four SINS galaxies by Cresci et al. (2009) at similar redshifts, it is consistent with no evolution of the zero point. These four galaxies are very massive ($\sim 10^{11} M_\odot$) with velocities around $\sim 250 \text{ km s}^{-1}$ where the two calibrations give similar estimates. At higher redshift, Cresci et al. (2009) found a shift in the stellar masses at fixed velocity of -0.41 ± 0.11 dex from the $z = 0$ Bell & de Jong (2001) calibration. Similar evolution is observed with the calibration of Pizagno et al. (2007), or -0.44 ± 0.11 dex (Cresci priv. comm.). The absence of any discrepancy when taking two different calibrations is expected giving the properties of the analysed SINS galaxies. They are very massive and fast rotators and are located at the intersection between the two local relations in the stellar mass - velocity diagram. Gnerucci et al. (2011) analysed the data set of LSD/AMAZE galaxies to discover evidence of the possible build-up of the stellar mass TF relation at $z \sim 3$. Despite the large scatter in the correlation (~ 1.5 dex), they report a statistical shift in the zero point relative to their local relation, of -1.29 dex (a very fast evolution, -0.88 dex, between $z \sim 2.2$ and 3 compared to more recent cosmic epochs).

Galaxies at high redshifts have a larger velocity dispersion and a higher fraction of turbulent motions (e.g., Genzel et al. 2008). To account for the large velocity dispersion that contributes to galactic kinematics at increasing redshift, we plot

in the bottom panel of Fig. 4 the relation between the stellar mass and the S_{05} index. The S_{05} index is defined as $S_{05} = \sqrt{0.5 \times v_{rot}^2 + \sigma_0^2}$ to account for the contributions of both ordered and turbulent motions (Kassin et al. 2007; Covington et al. 2010).

The cyan shaded area shows the 1σ error in the zero-point parameter, the cyan dotted and cyan dashed lines are the intrinsic and total scatters, respectively. The diagonal lines represent the best-fit relations of Kassin et al. (2007) at $z \sim 1$ (dot-dashed black line) and of Gnerucci et al. (2011) at $z \sim 3$ (dot-dashed magenta line) calibrated using the slope of Kassin et al. (2007). We found a tighter correlation that has a smaller scatter than the classical smTF relation. Physically this smaller scatter in the distribution reinforces the results on the importance of chaotic motions to the galactic kinematics, and the larger contamination encountered in traditional long-slit spectroscopy.

Using the S_{05} index, the rotators and non-rotators are located now in the same locus (bottom panel of Fig. 4). The $z \sim 1.2$ smTF $_{S05}$ is $\log(M_\star) = 4.46 \pm 0.07 + 2.92 \times \log(S_{05})$ (with $\sigma_{intr}=0.08$ and $\sigma_{tot}=0.45$) when galaxies of both classes are included. If only rotating galaxies are considered (this is the correlation plotted in the figure), the relation can be written as $\log(M_\star) = 4.26 \pm 0.10 + 2.92 \times \log(S_{05})$ (with $\sigma_{intr}=0.13$ and $\sigma_{tot}=0.43$). We therefore report a shift in stellar mass of -0.25 dex for the rotating MASSIV sample (or -0.45 dex including both dynamical classes) relative to the Kassin et al. (2007) galaxies at $z \sim 1$ and of $+0.35$ dex (or $+0.55$ dex) relative to the Gnerucci et al. (2011) galaxies at $z \sim 3$.

Figure 5 shows the relation between the baryonic mass and the velocities (top panel) and the ordered+chaotic motion components, quantified using the $S_{0.5}$ index (bottom panel). Based on our results, we infer that there has been no evolution which should be compared with the conclusions reached by McGaugh (2005) in the local Universe implying a very marginal evolution of the content of the gaseous component with respect to nearby galaxies. Previous results on the baryonic TF relation using a data-set of integral field survey were derived by Puech et al. (2010), who found no significant evolution compared to the local Universe.

These authors claimed that gas was already in place at $z \sim 0.6$ with no need to advocate external gas accretion since the gas was already bound to the gravity well of galaxies. Other interpretations are possible: if the predicted increases with cosmic time in both galactic velocities and masses occur according to the scaling relations, as predicted by LCDM models, any evolution should be observationally recognized.

6. Discussion and conclusions

We have explored the relationships between galaxy size, mass, and internal velocity of the statistically representative MASSIV sample of 45 galaxies with near-infrared resolved kinematics at $1 < z < 1.6$, an unbiased sample of high- z star-forming galaxies (Contini et al. 2012).

Before the advent of the three-dimensional integral field spectroscopy, the possible sources of discordance when using these quantities included observational difficulties and selection effects (Portinari & Sommer-Larsen 2007). The larger fraction of morphological and kinematic disturbances in high- z galaxies compared to nearby objects may bias the conclusions about the real evolutionary effects. However, systematics and subtle selection effects also need to be taken into account when comparing with recent near-infrared resolved kinematics surveys.

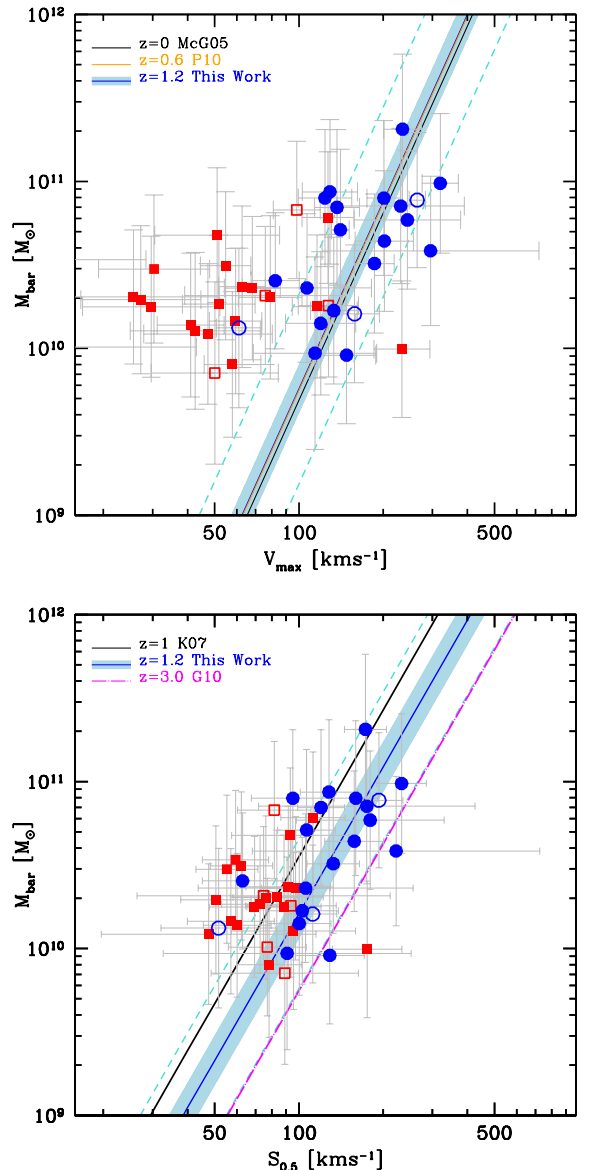


Fig. 5. The baryonic TF (bTF) relation versus the maximum velocity (top panel) and versus the $v + \sigma$ (or $S_{0.5}$) index (bottom panel). We overplot the best-fit relation of rotating galaxies (blue symbols) using the local slopes by McGaugh (2005) (plotted as solid black line in the top panel, McG05) and by Kassin et al. (2007) at $z \sim 1$ (plotted as solid black line in the bottom panel, K07). The other fit in the top panel is by Puech et al. (2010) (P10, $z \sim 0.6$, solid, orange line) and in the bottom panel by Gnerucci et al. (2011) ($z \sim 3$, long-dashed-dotted magenta line, G11). The cyan shaded area shows the 1σ error on the zero-point parameter (the intrinsic and total scatter is plotted as cyan dotted line and cyan dashed line, respectively). Symbols are as in Fig. 1.

For example, the observations of the OSIRIS sample (Law et al. 2007, 2009; Wright et al. 2008) were assisted by adaptive optics to reach very high angular resolutions, but probing only the highest surface brightness emission. With this observing mode, only smaller characteristic $H\alpha$ radii (~ 1.3 kpc) than those typically probed (~ 3 kpc) in other similar surveys at comparable redshifts could be studied. The IMAGES survey (Hammer et al.

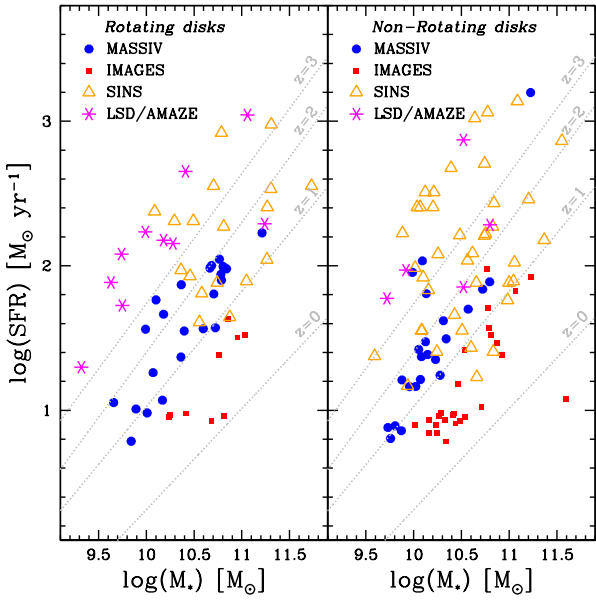


Fig. 6. Star formation rate versus stellar mass for rotators (left panel) and non-rotators (right panel) in the MASSIV ($1 < z < 1.6$, blue circle), IMAGES ($z \sim 0.6$, red square), SINS ($z \sim 2.2$, orange triangle), and LSD/AMAZE samples ($z \sim 3$, magenta asterisk). The grey dotted lines show the empirical main sequence of star-forming galaxies following Bouché et al. (2010) at different redshifts. All quantities have been rescaled to account for our Salpeter IMF.

2007; Puech et al. 2008, 2010) samples both star-forming and more quiescent galaxies, but the coarse spatial resolution of the FLAMES instrument requires meticulous correction methods to extract the maximum velocity. The SINS sample is the largest collection of galaxies of its kind at high- z , but is extracted from surveys with different selection criteria. The SINS sample used to analyse the relationship between stellar mass and velocity, represents galaxies detected with the highest S/N: they are the most luminous/massive, most rapidly rotating, and most highly star-forming galaxies.

In the left panel of Fig. 6, we present the implications of these observational findings for the physical interpretation, where the star formation rate of rotating discs obtained by SED fitting in resolved kinematics surveys is plotted as a function of the stellar mass. The class of non-rotating/merging systems is shown in the right panel of the same figure. The main sequence of star-forming galaxies defined by Bouché et al. (2010) is drawn at different redshifts. The IMAGES rotators lie below the sequence defined by the MASSIV rotators that was consistently rescaled to star formation rate and stellar mass at their later cosmic epoch (but covering a large interval of galactic properties), whereas similarly high- z LSD/AMAZE rotating discs stay above the sequence. The SINS rotators are highly star-forming objects and very massive, thus coincide with the massive, star-forming tail of the MASSIV galaxy distribution. The SINS properties can explain the mostly absent scatter in the Tully-Fisher relation by Cresci et al. (2009) relative to our scatter in the same relation (cf. our Fig. 4 with their Fig. 5). In contrast to our expectations, the difference in SFR between MASSIV and SINS galaxies cannot be attributed to the higher redshift and/or to the limits imposed on the minimum line flux to ensure detection (Contini et al. 2012). In this figure, there is a larger dispersion

in SINS rotators around the main sequence compared to other samples. This may be the consequence of at least two combined effects. The first cause may be the heterogeneous SINS selection. The second cause may be physical, and related to an unexpectedly larger incidence of internal/external mechanisms (inflows/mergers, outflows/feedback) acting on both the spectrophotometric and dynamical properties of rotating discs. While we cannot discard the second hypothesis, it is unlikely that the same mechanisms acting on SINS galaxies at $z \sim 2$ are not at play a few Gyr later in MASSIV galaxies (assuming both samples are representative of the entire rotating disc population). Nevertheless, we can speculate that we witness the same phenomena acting with different efficiencies in the various physical regimes (of galactic stellar mass, star-formation rate, etc.). Furthermore, comparing the SFR of rotators (left panel in Fig. 6) and non-rotators (right panel) for the SINS and MASSIV surveys, it appears that non-rotating systems display similar ranges of SFR at $z \sim 1$ and $z \sim 2$, while this is not the case for rotating systems that exhibit higher SFR at $z \sim 2$ than at $z \sim 1$. Our results highlight the importance of the disc formation to the SFR mechanics between $z \sim 2$ and $z \sim 1$. In summary, the galaxy datasets that have become available so far (even those taking advantage of resolved spectroscopy) are spectroscopic surveys that pass through a natural pre-selection from one, or several photometric catalogues. As a consequence, the comparison between samples remains difficult. At present, firm conclusions based on comparisons with other surveys that are affected in different ways by systematics in the galaxy properties determinations (e.g., different selection effects, quantities obtained at different wavelengths, and different assumptions), should be formulated with caution.

In this paper we have attempted a statistical analysis of our data set. We have analysed a large representative catalogue of galaxies with well-known selection functions, that is based on flux-limited multiple fields of a homogeneous redshift survey observed at higher spectral resolution, but with sufficient spatial resolution probing typical scales of ~ 5 kpc. Our results are the following.

The MASSIV galaxies show a correlation between dynamical and stellar mass with an offset between the two that can be interpreted as the gas mass being of the order of 20-25% of the stellar mass at $z \sim 1.2$. A similar fraction of gas mass is obtained using the Kennicutt-Schmidt formulation. We have found that this fraction of gas mass has evolved mildly for the past 8 Gyr, a result that is reinforced by the lack of a statistically significant evolution of our baryonic Tully-Fisher relation. In contrast, our finding of a disagreement in the gas estimates using two independent approaches for non-rotating galaxies, suggests different properties of dark matter halos between rotators and systems not supported by rotation at high- z , as is prescribed for nearby objects. The stellar mass in MASSIV galaxies is correlated with the incidence of being either a rotator or a non-rotator, with non-rotating galaxies containing a smaller amount of stellar mass at fixed gas content and dynamical mass, but not at fixed star-formation rate. Furthermore, non-rotators have more compact stellar components than rotators, but not for their gas components.

We have derived correlations between galaxy size, mass, and internal velocity, as observed in the local Universe and indicated by previous results, but the size - mass and size - velocity relations are weak at $1 < z < 1.6$. While individual galactic properties are found to evolve with time as advocated by the most recent results of large galaxy surveys, the marginal change ob-

served in the relationships linking the three fundamental quantities analysed in this work – size, mass, and internal velocity – suggests that there is some evolution in these relations. This picture agrees well with the cosmological N-body/hydrodynamical simulations by e.g., Portinari & Sommer-Larsen (2007) and Firmani & Avila-Reese (2009). We do not confirm the hypothesis of a strong, positive evolution in the size - stellar mass and size - velocity relations, where discs were found to be evenly smaller with look-back time at fixed stellar mass or velocity. Our results do not imply that there has been any unusual evolution in the galactic spin similar to that reported by Bouché et al. (2007). However, we have discovered a large spread in the distributions, which is significantly smaller for non-rotating galaxies when including the contribution of turbulent motions (with the S_{05} index) in the relations involving the velocities. This result disagrees with the hypothesis that large scatters in the low-velocity regime are due to disturbed or compact objects, as suggested by Covington et al. (2010). Restricting our analysis to regularly rotating discs that sample a large range of stellar masses and sizes, we have found that there is a persistent scatter. Its origin is likely intrinsic, and possibly caused by complex physical mechanism(s) at work in our stellar mass/luminosity regime and redshift range. At the present stage of the MASSIV survey and given the typical scale (~ 5 kpc) used to trace the resolved kinematics, we have been unable to investigate further the mechanism(s) driving these galactic properties. It is still a matter of debate as to whether we trace more turbulent discs where star formation is the energetic driver (e.g., Lehnert et al. 2009; Green et al. 2010), or we are influenced by the infall of accreting matter, and/or large collisional clumps (e.g., Law et al. 2007, 2009; Genzel et al. 2011), and/or merger events (e.g., Hammer et al. 2011).

More sophisticated analyses will be possible on the completion of our survey, doubling the statistics with galaxies in our highest ($z > 1.2$) redshift range. However, some problems will only be able to be addressed with larger-scale surveys of kinematically resolved galaxies. Future surveys should be able to assess firm conclusions about the cosmic evolution of the slope of the size/mass/velocity fundamental relations of discs at $z > 1$. There is also the pressing need to establish the imprint of the environmental processes at work in various stellar mass regimes. The stellar component and ionized gas content of galaxies of course offer only a partial view of galaxy formation and evolution, which must be supplemented with the properties of the cold/molecular phase of the interstellar component. In the future, we hope to comprehend under which conditions, and how efficiently, the gas is converted into stars through cosmic epochs. The relation between the galactic properties probed in our survey and the characteristics of the gas reservoir will offer a crucial step to link the data to models of galaxy formation.

7. Acknowledgments

DV acknowledges the support from the INAF contract PRIN-2008/1.06.11.02. This work has been partially supported by the CNRS-INSU and its Programme National Cosmologie-Galaxies (France) and the French ANR grant ANR-07-JCJC-0009.

References

Arnouts, S., Walcher, C. J., Le Fèvre, O., et al. 2007, *A&A*, 476, 137
 Baker, A. J., Tacconi, L. J., Genzel, R., Lehnert, M. D., & Lutz, D. 2004, *ApJ*, 604, 125
 Bamford, S. P., Milvang-Jensen, B., & Aragón-Salamanca, A. 2007, *MNRAS*, 378, L6
 Bell, E. F. & de Jong, R. S. 2001, *ApJ*, 550, 212
 Bell, E. F., McIntosh, D. H., Katz, N., & Weinberg, M. D. 2003, *ApJS*, 149, 289
 Blumenthal, G. R., Faber, S. M., Primack, J. R., & Rees, M. J. 1984, *Nature*, 311, 517
 Bonnet, H., Abuter, R., Baker, A., et al. 2004, *The Messenger*, 117, 17
 Bouché, N., Cresci, G., Davies, R., et al. 2007, *ApJ*, 671, 303
 Bouché, N., Dekel, A., Genzel, R., et al. 2010, *ApJ*, 718, 1001
 Bruzual, G. & Charlot, S. 2003, *MNRAS*, 344, 1000
 Bundy, K., Ellis, R. S., Conselice, C. J., et al. 2006, *ApJ*, 651, 120
 Conselice, C. J., Bundy, K., Ellis, R. S., et al. 2005, *ApJ*, 628, 160
 Contini, T., Garilli, B., Le Fèvre, O., et al. 2012, *A&A*, 539, A91
 Courteau, S. 1997, *AJ*, 114, 2402
 Covington, M. D., Kassin, S. A., Dutton, A. A., et al. 2010, *ApJ*, 710, 279
 Cowie, L. L., Songaila, A., Hu, E. M., & Cohen, J. G. 1996, *AJ*, 112, 839
 Cresci, G., Hicks, E. K. S., Genzel, R., et al. 2009, *ApJ*, 697, 115
 Cucciati, O., Tresse, L., Ilbert, O., et al. 2012, *A&A*, 539, A31
 Daddi, E., Bournaud, F., Walter, F., et al. 2010, *ApJ*, 713, 686
 Dalcanton, J. J., Spergel, D. N., & Summers, F. J. 1997, *ApJ*, 482, 659
 de Jong, R. S. & Lacey, C. 2000, *ApJ*, 545, 781
 Dekel, A., Birnboim, Y., Engel, G., et al. 2009, *Nature*, 457, 451
 Dutton, A. A., van den Bosch, F. C., Dekel, A., & Courteau, S. 2007, *ApJ*, 654, 27
 Dutton, A. A., van den Bosch, F. C., Faber, S. M., et al. 2011, *MNRAS*, 410, 1660
 Eisenhauer, F., Abuter, R., Bickert, K., et al. 2003, in *Society of Photo-Optical Instrumentation Engineers (SPIE) Conference Series*, Vol. 4841, *Society of Photo-Optical Instrumentation Engineers (SPIE) Conference Series*, ed. M. Iye & A. F. M. Moorwood, 1548–1561
 Epinat, B., Amram, P., & Marcelin, M. 2008, *MNRAS*, 390, 466
 Epinat, B., Contini, T., Le Fèvre, O., et al. 2009, *A&A*, 504, 789
 Epinat, B., Tasca, L., Amram, P., et al. 2012, *A&A*, 539, A92
 Erb, D. K., Steidel, C. C., Shapley, A. E., et al. 2006, *ApJ*, 646, 107
 Fernández Lorenzo, M., Cepa, J., Bongiovanni, A., et al. 2010, *A&A*, 521, A27+
 Firmani, C. & Avila-Reese, V. 2000, *MNRAS*, 315, 457
 Firmani, C. & Avila-Reese, V. 2009, *MNRAS*, 396, 1675
 Flores, H., Hammer, F., Puech, M., Amram, P., & Balkowski, C. 2006, *A&A*, 455, 107
 Fontana, A., Pozzetti, L., Donnarumma, I., et al. 2004, *A&A*, 424, 23
 Fontana, A., Salimbeni, S., Grazian, A., et al. 2006, *A&A*, 459, 745
 Förster Schreiber, N. M., Genzel, R., Bouché, N., et al. 2009, *ApJ*, 706, 1364
 Förster Schreiber, N. M., Genzel, R., Lehnert, M. D., et al. 2006, *ApJ*, 645, 1062
 Franzetti, P., Scoggio, M., Garilli, B., Fumana, M., & Paioro, L. 2008, in *Astronomical Society of the Pacific Conference Series*, Vol. 394, *Astronomical Data Analysis Software and Systems XVII*, ed. R. W. Argyle, P. S. Bunclark, & J. R. Lewis, 642–+
 Garilli, B., Le Fèvre, O., Guzzo, L., et al. 2008, *A&A*, 486, 683
 Garrido, O., Marcelin, M., Amram, P., et al. 2005, *MNRAS*, 362, 127
 Genel, S., Genzel, R., Bouché, N., et al. 2008, *ApJ*, 688, 789
 Genzel, R., Burkert, A., Bouché, N., et al. 2008, *ApJ*, 687, 59
 Genzel, R., Newman, S., Jones, T., et al. 2011, *ApJ*, 733, 101
 Genzel, R., Tacconi, L. J., Eisenhauer, F., et al. 2006, *Nature*, 442, 786
 Gnerucci, A., Marconi, A., Cresci, G., et al. 2011, *A&A*, 528, A88+
 Green, A. W., Glazebrook, K., McGregor, P. J., et al. 2010, *Nature*, 467, 684
 Hammer, F., Puech, M., Chemin, L., Flores, H., & Lehnert, M. D. 2007, *ApJ*, 662, 322
 Hammer, F., Puech, M., Flores, H., et al. 2011, in *SF2A-2011: Proceedings of the Annual meeting of the French Society of Astronomy and Astrophysics*, ed. G. Alecian, K. Belkacem, R. Samadi, & D. Valls-Gabaud, 135–140
 Kassin, S. A., Weiner, B. J., Faber, S. M., et al. 2007, *ApJ*, 660, L35
 Kennicutt, R. C. 1998a, *ARA&A*, 36, 189
 Kennicutt, Jr., R. C. 1998b, *ApJ*, 498, 541
 Larkin, J., Barcys, M., Krabbe, A., et al. 2006, *New Astronomy Review*, 50, 362
 Law, D. R., Steidel, C. C., Erb, D. K., et al. 2007, *ApJ*, 669, 929
 Law, D. R., Steidel, C. C., Erb, D. K., et al. 2009, *ApJ*, 697, 2057
 Le Fèvre, O., Vettolani, G., Garilli, B., et al. 2005, *A&A*, 439, 845
 Lehnert, M. D., Nesvadba, N. P. H., Tiran, L. L., et al. 2009, *ApJ*, 699, 1660
 Markwardt, C. B. 2009, in *Astronomical Society of the Pacific Conference Series*, Vol. 411, *Astronomical Data Analysis Software and Systems XVIII*, ed. D. A. Bohlender, D. Durand, & P. Dowler, 251
 Mathewson, D. S., Ford, V. L., & Buchhorn, M. 1992, *ApJS*, 81, 413
 McCracken, H. J., Radovich, M., Bertin, E., et al. 2003, *A&A*, 410, 17
 McGaugh, S. S. 2005, *ApJ*, 632, 859
 Meurer, G. R., Carignan, C., Beaulieu, S. F., & Freeman, K. C. 1996, *AJ*, 111, 1551
 Mo, H. J., Mao, S., & White, S. D. M. 1998, *MNRAS*, 295, 319
 Modigliani, A., Hummel, W., Abuter, R., & et al. 2007, *ArXiv e-prints*
 Noordermeer, E. & Verheijen, M. A. W. 2007, *MNRAS*, 381, 1463

Peng, C. Y., Ho, L. C., Impey, C. D., & Rix, H.-W. 2002, AJ, 124, 266

Persic, M. & Salucci, P. 1991, ApJ, 368, 60

Persic, M., Salucci, P., & Stel, F. 1996, MNRAS, 281, 27

Pizagno, J., Prada, F., Weinberg, D. H., et al. 2005, ApJ, 633, 844

Pizagno, J., Prada, F., Weinberg, D. H., et al. 2007, AJ, 134, 945

Portinari, L. & Sommer-Larsen, J. 2007, MNRAS, 375, 913

Pozzetti, L., Bolzonella, M., Lamareille, F., et al. 2007, A&A, 474, 443

Puech, M., Flores, H., Hammer, F., et al. 2008, A&A, 484, 173

Puech, M., Hammer, F., Flores, H., et al. 2010, A&A, 510, A68+

Puech, M., Hammer, F., Lehnert, M. D., & Flores, H. 2007, A&A, 466, 83

Queyrel, J., Contini, T., Kissler-Patig, M., et al. 2011, ArXiv e-prints

Robertson, B. E. & Bullock, J. S. 2008, ApJ, 685, L27

Rodrigues, M., Hammer, F., Flores, H., et al. 2008, A&A, 492, 371

Salpeter, E. E. 1955, ApJ, 121, 161

Schiminovich, D. 2008, in American Institute of Physics Conference Series, Vol. 1035, The Evolution of Galaxies Through the Neutral Hydrogen Window, ed. R. Minchin & E. Momjian, 180–185

Schmidt, M. 1959, ApJ, 129, 243

Stark, D. P., Swinbank, A. M., Ellis, R. S., et al. 2008, Nature, 455, 775

Tacconi, L. J., Genzel, R., Neri, R., et al. 2010, Nature, 463, 781

Tresse, L., Ilbert, O., Zucca, E., et al. 2007, A&A, 472, 403

Trujillo, I., Förster Schreiber, N. M., Rudnick, G., et al. 2006, ApJ, 650, 18

Tully, R. B. & Fisher, J. R. 1977, A&A, 54, 661

Vergani, D., Scudeggi, M., Pozzetti, L., et al. 2008, A&A, 487, 89

Verheijen, M. A. W. 2001, ApJ, 563, 694

Walcher, C. J., Lamareille, F., Vergani, D., et al. 2008, A&A, 491, 713

Weiner, B. J., Willmer, C. N. A., Faber, S. M., et al. 2006, ApJ, 653, 1049

Williams, R. J., Quadri, R. F., Franx, M., et al. 2010, ApJ, 713, 738

Wright, S. A., Larkin, J. E., Law, D. R., et al. 2008, in Astronomical Society of the Pacific Conference Series, Vol. 396, Formation and Evolution of Galaxy Disks, ed. J. G. Funes & E. M. Corsini, 433

Zucca, E., Ilbert, O., Bardelli, S., et al. 2006, A&A, 455, 879